Department of Applied Physics

Development and applications of multi-physics capabilities in a continuous energy Monte Carlo neutron transport code

Ville Valtavirta

Aalto University

DOCTORAL DISSERTATIONS

Aalto University publication series
DOCTORAL DISSERTATIONS 66/2017
VTT SCIENCE 150

Development and applications of multi-physics capabilities in a continuous energy Monte Carlo neutron transport code

Ville Valtavirta

A doctoral dissertation completed for the degree of Doctor of Science (Technology) to be defended, with the permission of the Aalto University School of Science, at a public examination held at the lecture hall E of the school on 19. 5. 2017 at 13:00.

Aalto University
School of Science
Department of Applied Physics

Supervising professor
Prof. Filip Tuomisto, Aalto University, Finland

Thesis advisor
Adj. Prof. Jaakko Leppänen, VTT Technical Research Centre of Finland Ltd

Preliminary examiners
Dr. Kevin T. Clarno, Oak Ridge National Laboratory, United States of America
Assist. Prof. Dan Kotlyar, Georgia Institute of Technology, United States of America

Opponent
Dr. Mark DeHart, Idaho National Laboratory, United States of America

Aalto University publication series
DOCTORAL DISSERTATIONS 66/2017

VTT SCIENCE 150

ISBN 978-952-60-7377-4 (printed)
ISBN 978-952-60-7376-7 (pdf)
ISSN-L 1799-4934
ISSN 1799-4934 (printed)
ISSN 1799-4942 (pdf)
http://urn.fi/URN:ISBN:978-952-60-7376-7

ISBN 978-951-38-8530-4 (printed)
ISBN 978-951-38-8529-8 (pdf)
ISSN-L 2242-119X
ISSN 2242-119X (printed)
ISSN 2242-1203 (pdf)
http://urn.fi/URN:ISBN:978-951-38-8529-8

Unigrafia Oy
Helsinki 2017

Finland

441 697
Printed matter

Aalto University

Abstract

Aalto University, P.O. Box 11000, FI-00076 Aalto www.aalto.fi

Author
Ville Valtavirta

Name of the doctoral dissertation
Development and applications of multi-physics capabilities in a continuous energy Monte Carlo neutron transport code

Publisher School of Science

Unit Department of Applied Physics

Series Aalto University publication series DOCTORAL DISSERTATIONS 66/2017

Field of research Engineering Physics

Manuscript submitted 28 November 2015 **Date of the defence** 19 May 2017

Permission to publish granted (date) 8 March 2017 **Language** English

☐ **Monograph** ☒ **Article dissertation** ☐ **Essay dissertation**

Abstract

The accurate modeling of nuclear reactors is essential to the safe and economic operation of current and future reactor types. Due to the physical feedback effects between the neutron distribution in the reactor core and the fuel and coolant material temperatures and densities, all of the three fields need to be solved simultaneously in order to obtain a solution for the behavior of the nuclear reactor. This coupled problem has traditionally been solved using a two-stage approach for the neutron transport. In this approach, the neutron interaction properties of different parts of the reactor core are first averaged using accurate neutron transport methods in a series of small scale simulations. These averaged quantities are then used in a simplified neutron transport model to obtain the full-core solution in a reasonable time allowing for multiple iterations between the solvers of the different physical fields.

In recent years, advances in methodology as well as in computational power have made it possible to apply the accurate neutron transport methods directly to the full core problem, enabling modeling of the important feedback effects in more detail than has been possible with the two-stage approach. Moving to direct modeling of the coupled problem with the accurate neutron transport methods initially developed for the lattice calculations in the first part of the two-stage approach requires various changes to the neutron transport methods.

In this thesis, capabilities required to solve the neutron transport part of the coupled problem are developed and implemented in the continuous energy Monte Carlo neutron transport code Serpent 2. Coupled calculation schemes were developed and implemented both for internally and externally coupled calculations for three different simulation types: Steady state calculations, burnup calculations and time-dependent transient calculations.

The new coupled calculation capabilities were applied to the effective fuel temperature approximation, in which the complex fuel temperature distribution in a fuel rod or a fuel assembly is replaced with a single effective temperature for the neutron transport calculations. The new capabilities made it possible to estimate the effects of this approximation by providing an accurate reference solution using realistic temperature distributions provided by an internally or externally coupled fuel temperature solver.

Keywords Neutron transport, Monte Carlo, multi-physics, coupled calculation, reactor analysis

ISBN (printed) 978-952-60-7377-4 **ISBN (pdf)** 978-952-60-7376-7

ISSN-L 1799-4934 **ISSN (printed)** 1799-4934 **ISSN (pdf)** 1799-4942

Location of publisher Helsinki **Location of printing** Helsinki **Year** 2017

Pages 172 **urn** http://urn.fi/URN:ISBN:978-952-60-7376-7

Aalto-yliopisto

Tiivistelmä

Aalto-yliopisto, PL 11000, 00076 Aalto www.aalto.fi

Tekijä
Ville Valtavirta

Väitöskirjan nimi
Multifysiikkamenetelmien kehitys ja sovellukset jatkuvaenergisessä Monte Carlo neutronikuljetuskoodissa

Julkaisija Perustieteiden korkeakoulu

Yksikkö Teknillisen fysiikan laitos

Sarja Aalto University publication series DOCTORAL DISSERTATIONS 66/2017

Tutkimusala Teknillinen fysiikka

Käsikirjoituksen pvm 28.11.2015 **Väitöspäivä** 19.05.2017

Julkaisuluvan myöntämispäivä 08.03.2017 **Kieli** Englanti

☐ **Monografia** ☒ **Artikkeliväitöskirja** ☐ **Esseeväitöskirja**

Tiivistelmä
Tiivistelmä
Neutronien käyttäytymisen ja reaktorisydämen materiaalien lämpötilan ja tiheyden välillä olevat fysikaaliset takaisinkytkennät tekevät reaktorimallinnuksesta kytketyn ongelman: reaktorisydämen tehojakauman ratkaisemiseksi täytyy samanaikaisesti ratkaista myös jäähdytteen ja polttoaineen lämpötila- ja tiheysjakaumat. Menetelmiltä vaaditun lyhyen laskenta-ajan vuoksi neutronien käyttäytyminen ratkaistaan tyypillisesti käyttäen kaksivaiheista laskentaketjua. Ketjun ensimmäisessä osassa reaktorisydämen eri alueille lasketaan tarkoilla menetelmillä joukko neutronien vuorovaikutuksia kuvaavia keskiarvoistettuja parametreja. Toisessa vaiheessa näitä keskiarvoistettuja suureita käytetään yksinkertaistetussa mutta nopeassa koko reaktorisydämen kattavassa laskentamallissa.

Viime vuosina laskentamenetelmien ja käytettävissä olevan laskentatehon kehitys on tehnyt mahdolliseksi soveltaa ensimmäisen vaiheen tarkkoja neutronilaskentamenetelmiä suoraan kokosydänongelmaan. Näitä menetelmiä ei kuitenkaan ole alun perin kehitetty kytketyn ongelman ratkaisemiseen, mikä vaatii uusien toiminnallisuuksien kehittämistä ja toteuttamista.

Tässä väitöskirjassa kehitettiin kytketyn ongelman ratkaisemiseen vaadittavat laskentamenetelmät Serpent 2 nimiseen jatkuvaenergiseen Monte Carlo neutronikuljetuskoodiin. Työn valmistuttua Serpent 2 pystyy ratkaisemaan kytketyn ongelman neutroniikkaosuuden osana laskentajärjestelmää, jossa toiset Serpentiin sisäisesti tai ulkoisesti kytketyt ratkaisijat vastaavat lämpötila ja tiheyskenttien ratkaisusta. Kytkettyyn laskentaan kehitetyt menetelmät soveltuvat ajasta riippumattomien laskujen lisäksi palamalaskentaan ja aikariippuvaan transienttilaskentaan.

Väitöskirjassa kehitettyjä laskentamenetelmiä käytettiin esimerkkisovelluksena ydinpolttoaineen efektiivisen lämpötilan tutkimiseen. Nipputason neutronikuljetuslaskuissa tyypillisesti käytettävä yksinkertaistus on korvata ydinpolttoaineen monimutkainen lämpötilajakauma yhdellä efektiivisellä lämpötilalla, joka valitaan siten että mallinnuksesta saatavat tulokset vastaisivat mahdollisimman hyvin oikealla lämpötilaprofiililla saatavia tuloksia. Uudet menetelmät mahdollistivat tarkan vertailuratkaisun laskemisen oikeaa lämpötilaprofiilia käyttäen ja efektiivisten lämpötilamallien vaikutusten arvioinnin.

Avainsanat Neutronikuljetus, Monte Carlo, multifysiikka, kytketyt ongelmat, reaktorimallinnus

ISBN (painettu) 978-952-60-7377-4 **ISBN (pdf)** 978-952-60-7376-7

ISSN-L 1799-4934 **ISSN (painettu)** 1799-4934 **ISSN (pdf)** 1799-4942

Julkaisupaikka Helsinki **Painopaikka** Helsinki **Vuosi** 2017

Sivumäärä 172 **urn** http://urn.fi/URN:ISBN:978-952-60-7376-7

Preface

I want to express my appreciation for everything that my instructor Dr. Jaakko Leppänen has provided me with. Not only did he offer me a stimulating topic for my postgraduate research and funding to follow through with it, he has also both created a Monte Carlo code that is extremely nice to work with and been a key factor in bringing together a group of young motivated researchers, who also happen to be extremely nice to work with.

On this note, I would like to thank all of my colleagues at VTT who have served as my surrogate family for some 36.25 or, more recently, 37.5 hours a week. I want to extend special thanks to the people who have accompanied me on, and whom I have met in, various conference and Serpent UGM travels. Many of the most memorable moments of my PhD candidacy are from those trips.

For the support I have received at VTT, I also want to thank my team leader Petri Kotiluoto and the former Head of Research Area Timo Vanttola.

I want to thank four specific doctors of technology, Jaana Vapaavuori, Maria Pusa, Tuomas Viitanen and Eric Dorval, whom I have had the pleasure to work with and whose journeys towards their PhD's have inspired me on my own.

I am grateful for my two professors from the Department of Applied Physics in Aalto University: Professor Emeritus Rainer Salomaa, who encouraged me to pursue a PhD and Professor Filip Tuomisto who has acted as my supervisor during these years.

I was delighted to hear that Dr. Mark DeHart from Idaho National Laboratory agreed to serve as my opponent in the defense of this thesis and I thank him for accepting this task. I also want to express my gratitude for my two pre-examiners Dr. Kevin T. Clarno from Oak Ridge National Laboratory and Dr. Dan Kotlyar from the Georgia Institute of Technology. Their comments and suggestions were of great value in the final phase of preparing my dissertation.

My parents have had an enormous role in feeding my thirst for knowledge all through my childhood and education. I fondly remember our frequent visits to the local library that we often conducted by bike. The access to a vast amount of interesting books and the encouragement I received for reading has surely shaped me from an early age.

I am grateful to my wife Anna-Maija, whose musings on how it is preferable to do difficult things and feel like one gets a bit smarter every day than to do easy things and feel like one gets a bit more dumb each day bring me solace whenever I'm trying to tackle advanced topics myself.

Finally, I want to thank our dog Susu who helped me in the final phase of my thesis work by taking a vacation and living in Vaasa with my parents, so that I could focus on the writing process.

This work has been funded by the Finnish Academy project NUMPS, the Finnish Research Programme on Nuclear Power Plant Safety SAFIR and the Fortum Foundation.

List of publications

This thesis is based on the following original publications which are referred to in the text as **I**–**VI**. The publications are reproduced with kind permission from the publishers.

I V. VALTAVIRTA, T. VIITANEN and J. LEPPÄNEN, "Internal neutronics–temperature coupling in Serpent 2", *Nuclear Science and Engineering*, **177**, pp. 193-202 (2014).

II V. VALTAVIRTA, V. TULKKI, J. LEPPÄNEN and T. VIITANEN, "The universal fuel performance code interface in Serpent 2", *In proc.* TopFuel 2013, Charlotte, NC, Sept. 15–19, 2013, (2013).

III V. VALTAVIRTA, T. IKONEN, T. VIITANEN and J. LEPPÄNEN, "Simulating fast transients with fuel behavior feedback using the Serpent 2 Monte Carlo code", *In proc.* PHYSOR 2014, Kyoto, Japan, Sept. 28–Oct. 3, 2014, (2014).

IV V. VALTAVIRTA, M. HESSAN and J. LEPPÄNEN, "Delayed neutron emission model for time dependent simulations with the Serpent 2 Monte Carlo code – first results", *In proc.* PHYSOR 2016, Sun Valley, ID, May 1–5, 2016, (2016).

V V. VALTAVIRTA, J. LEPPÄNEN and T. VIITANEN, "Coupled neutronics–fuel behavior calculations in steady state using the Serpent 2 Monte Carlo code", *Annals of Nuclear Energy*, **100, Part 2**, pp. 50–64 (2017).

VI V. VALTAVIRTA and J. LEPPÄNEN, "Estimating the effects of homogenized fuel temperature in group constant generation using Serpent 2", *Annals of Nuclear Energy*, **105**, pp. 79–94 (2017).

Author's contribution

Publication I: Internal neutronics–temperature coupling in Serpent 2

The author designed and implemented the internal analytic fuel temperature solver and coupled calculation scheme described in the article, chose the test problem, conducted all the simulations, analyzed the results and was the main author of the article.

Publication II: The universal fuel performance code interface in Serpent 2

The author designed and implemented the general fuel performance code interface described in the article as well as the coupled calculation routines needed for the external coupling, chose the test case, conducted the simulations, analyzed the results and was the main author of the article.

Publication III: Simulating fast transients with fuel behavior feedback using the Serpent 2 Monte Carlo code

The author designed and implemented the internal coupling with the FINIX fuel behavior module as well as the solution procedure for the coupled time-dependent simulation described in the article. The author also chose the time-dependent test problem, conducted the simulation, analyzed the results and was the main author of the article.

Publication IV: Delayed neutron emission model for time dependent simulations with the Serpent 2 Monte Carlo code – first results

The author developed the mesh-based precursor tracking in collaboration with the third author of the article and implemented the methodology described in the article for source generation, precursor tracking and conducting time-dependent simulations with delayed neutrons. The author chose the test case, conducted the simulations, analyzed the results and was the main author of the article.

Publication V: Coupled neutronics–fuel behavior calculations in steady state using the Serpent 2 Monte Carlo code

The author designed and implemented the coupled calculation schemes for external and internal coupling described in the article. The author chose the test case, conducted the simulations, analyzed the results and was the main author of the article.

Publication VI: Estimating the Effects of Homogenized Fuel Temperature in Group Constant Generation using Serpent 2

The author implemented the Stochastic Implicit Euler depletion scheme with thermal feedback into Serpent. The author also designed and implemented the coupled calculation routines Serpent required for the externally coupled burnup calculation. The author chose the test case, conducted the simulations, analyzed the results and was the main author of the article.

Contents

List of symbols and abbreviations

Symbols:

E	: Neutron energy.
v	: Neutron speed, scalar variable.
$\vec{v}$	: Neutron velocity, vector variable
$\hat{\Omega}$	: Direction of neutron movement: $\vec{v} = \hat{\Omega} v$
m_n	: Neutron mass.
ϕ	: Scalar neutron flux
σ_r^n	: Microscopic cross section for reaction r with material or nuclide n.
Σ_r^n	: Macroscopic cross section for reaction r with material or nuclide n.
$\dot{r}_x$	: Reaction rate density for reaction x.
$\dot{R}_x$	: Reaction rate for reaction x.
$k_{\text{eff.}}$	: Effective multiplication factor
s	: Neutron track length between two interactions.

Abbreviations:

BWR	: Boiling water reactor
CDF	: Cumulative distribution function
IQS	: Improved Quasi-Static
JEFF	: Joint European Fission and Fusion File
JFNK	: Jacobian-free Newton–Krylov
LEU	: Low enriched uranium
LFR	: Lead-cooled fast reactor
LWR	: Light water reactor
MC	: Monte Carlo
MOX	: Mixed oxide
PDF	: Probability density function
PWR	: Pressurized water reactor
SFR	: Sodium-cooled fast reactor
SIE	: Stochastic implicit Euler
TMS	: Target Motion Sampling
VVER	: A PWR design originally developed in the Soviet Union

1. Introduction

Power production in nuclear fission reactors is based on a stable neutron chain reaction, in which the power and neutrons are supplied by the neutron-induced fission of heavy elements, typically uranium-235. The combination of nuclear power's low lifetime greenhouse gas emissions for electricity generation (see Chapter 7 in [1]) and the strong load-following capabilities of both current and future reactor types [2] ensures that nuclear power can be used in conjunction with intermittent energy sources such as wind and solar power to tackle the continuing problem of increasing global greenhouse gas emissions.

In order to operate nuclear reactors in a safe and economic manner, it is imperative to understand accurately the behavior of the reactor, both in normal operating conditions and in accident scenarios. As it is both difficult and expensive to conduct experiments with full-sized reactors, such experiments are complemented with experiments executed in test reactors as well as with numerical simulations. Since power generation is based on the neutron chain reaction, accurate modeling of the neutron distribution in the reactor core is of great importance.

Safe reactor design relies on using the natural laws of neutron interactions with matter to design the reactor in such a way that physical laws ensure the existence of a *negative power feedback* in the reactor. This means that an increase in the reactor power should bring about feedback effects that oppose the increase in reactor power and vice versa. In thermal reactors, the negative power feedback effect is based on designs in which an increase in the fuel or coolant temperature will affect the power level in a decreasing manner.

The strong coupling between the power distribution and the material temperatures in the reactor core makes the reactor safe to operate, but difficult to model: For example, solving the power distribution in the reactor using a neutron transport tool requires a solution for the fuel and coolant temperature distributions as input data. However, the temperature distributions can only be solved if the power distribution is already known. This is the two-way coupled multi-physics problem in nuclear reactor modeling. Accounting for the feedback effects in the neutron transport solution transforms the neutron transport problem from a straightforward linear problem into a complex coupled non-linear one.

Traditionally, the coupled problem has been too costly to be solved using high-fidelity neutron transport methods. Instead, a two-level calculation approach has been used, in which the neutron interaction properties of a fuel assembly are first evaluated by an accurate lattice transport code for several different state points. These properties are then parametrized as the function of different thermal-hydraulic states and used in a coarser full-core simulator that only sees the neutron interactions through the pre-generated data.

Although the daily work of multi-physics calculations will continue to be conducted with simplified neutronics models in the future, application of the accurate continuous energy Monte Carlo neutron transport codes to multi-physics problems has increased in popularity during the past decade (see, e.g., [3], [4], [5], [6], [7]). Despite their high computational cost the Monte Carlo codes hold several advantages over simpler nodal solvers: The same code can naturally model different reactor and fuel types, no major approximations are made in the neutron physics models and the best possible interaction physics data can be used in the calcula-

tions. These features are important especially in new reactor concepts, in which the accuracy of the traditional two-level approach cannot be established by comparisons to experimental data.

Most Monte Carlo neutron transport codes have not originally been developed with multi-physics problems in mind, which means that the increased interest in the topic has necessitated the implementation of various new models in Monte Carlo codes. The models mainly focus on treatment of the complex temperature and density fields that appear in the multi-physics problem and on operation of the code in a coupled manner as a part of a larger multi-physics framework consisting of several solvers for the different physics fields.

The main topic of this thesis is the development and implementation of several new multi-physics and coupled calculation capabilities for the continuous energy Monte Carlo code Serpent 2 [8]. The implemented capabilities were demonstrated in various coupled calculation scenarios involving the coupling between the neutron flux and the fuel temperature. This work is described in Publications **I**–**VI** and summarized shortly in Sections 7 and 8. The physical and theoretical background of the multi-physics problem in the context of Monte Carlo neutron transport is briefly described in Sections 2–6.

Although the demonstration calculations in Publications **I**–**VI** focus on the neutronics–fuel temperature coupling, the capabilities developed in this thesis are by no means limited to the fuel behavior feedback.

2. Basics of neutron interactions with matter

This section will present and define some basic concepts that are required in order to understand the Monte Carlo neutron transport described in Section 3 as well as the description of the operation of thermal nuclear reactors given in Section 4.

2.1 Cross sections

Free neutrons travel in straight lines[1] at a velocity v determined by their kinetic energy E. These straight neutron tracks can be interrupted by interactions with matter. There are several possible interactions between neutrons and atomic nuclei, some of which will be introduced in Section 2.3. The probability for a neutron to interact with a specific nuclide via a specific reaction type depends on the nuclide, the reaction type and the neutron energy. These interaction probabilities are referred to as nuclear *cross sections*. The next sections will briefly describe the concept of macroscopic and microscopic nuclear cross sections.

2.1.1 Macroscopic cross sections

The probability for a neutron to interact with matter is strongly dependent on the neutron's energy and the composition of the material. The material total macroscopic cross section $\Sigma_t(E)$ describes the probability of a neutron with energy E to interact with the material when it travels a differential track-length ds in the material:

$$\frac{dP(E)}{ds} = \Sigma_t(E). \tag{1}$$

Based on this definition, the unit of macroscopic cross section is $1/\text{cm}$. The macroscopic total cross section can be divided into components: As the total interaction probability must be the sum of the interaction probabilities with each nuclide in the material composition, we can divide the material total macroscopic cross section into parts based on the target nuclide. For example, the total macroscopic cross section for light water H_2O will be the sum of the macroscopic cross sections of ^{1}H and the oxygen isotopes:

$$\Sigma_t^{H_2O} = \Sigma_t^{^1H} + \Sigma_t^{^{16}O} + \Sigma_t^{^{17}O} + \Sigma_t^{^{18}O}. \tag{2}$$

The quantity $\Sigma_t^{^1H}$ then represents the interaction probability with hydrogen-1 on the differential track-length ds. The nuclide-wise interaction probabilities can be further divided into interaction probabilities for the different reaction types:

$$\Sigma_t^{^1H} = \Sigma_s^{^1H} + \Sigma_c^{^1H}, \tag{3}$$

i.e. the probability for the neutron to interact with ^{1}H in any way on the differential track-length is the sum of the probabilities for a scattering reaction and a capture reaction with ^{1}H on the track-length. The material total macroscopic cross section is

[1] The effect of gravity on neutron trajectories can be ignored in reactor applications.

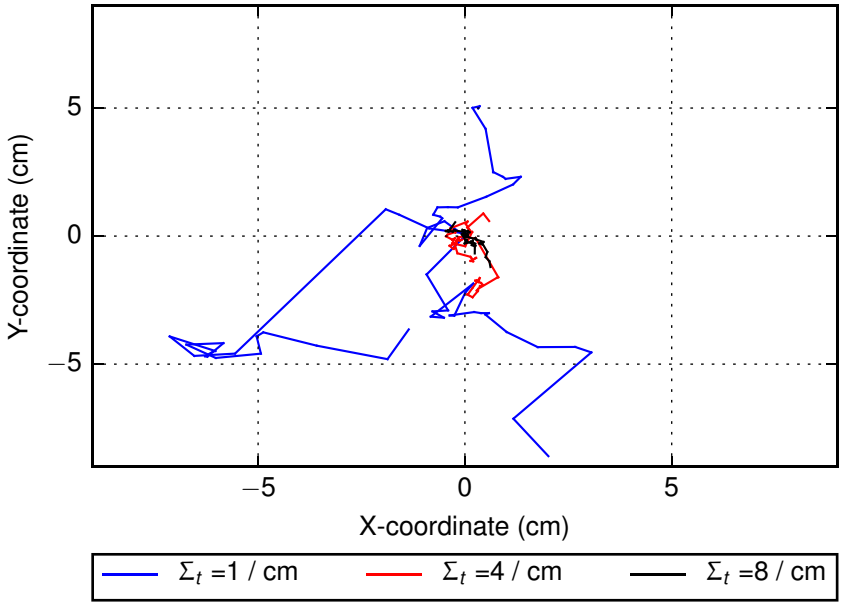

Figure 1. 2D projections of 3D particle tracks in a medium consisting of a pure isotropic scatterer with three different material total macroscopic cross sections. Increasing macroscopic total cross section leads, on average, to shorter track-lengths between scattering interactions. Three particle tracks were sampled for each Σ_t starting from (0,0) with 20 interactions for each particle track. Due to the projection of the tracks to the XY-plane, the segments traveling significant distances in the Z-direction are shortened.

then the sum of the nuclide total macroscopic cross sections, which themselves are the sums of the different reaction cross sections for the nuclide:

$$\Sigma_t = \sum^{\text{nuclides}} \left[\sum^{\text{reactions}} \Sigma_r^n \right]. \tag{4}$$

As the material total macroscopic cross section describes the interaction probability over an infinitesimal track-length, Eq. 1 can be used to derive an expression for the probability density function for the track-length (or path-length) between two interactions in an infinite homogeneous medium. The derivation can be found in most reactor physics textbooks such as [9, 10], and the resulting probability density function (PDF) has the simple form:

$$\mathbb{P}(E, s) = \Sigma_t(E) e^{-s\Sigma_t(E)}, \tag{5}$$

where s is the track-length between two interactions. This PDF can be used to obtain the expected value for the track-length, which is called the *mean-free-path* of

neutrons of energy E in the material:

$$l(E) = \int_0^\infty s\mathbb{P}(E,s)\mathrm{d}s = \int_0^\infty s\Sigma_t(E)e^{-s\Sigma_t(E)}\mathrm{d}s, \tag{6}$$

where the integral can be evaluated using integration by parts to yield

$$l(E) = \frac{1}{\Sigma_t(E)}. \tag{7}$$

The expected value for the track-length at energy E is thus the inverse of the material macroscopic total cross section at energy E. The effect of Σ_t on the track-length distribution is illustrated in Fig. 1, which shows track-lengths sampled for particles in three purely scattering materials with different macroscopic cross sections. Larger Σ_t corresponds on average to shorter track-lengths.

The macroscopic cross section (interaction probability) of each nuclide is a macroscopic property in the sense that it scales linearly with the number density of the nuclide. The interaction probability over an infinitesimal track-length in helium gas at $2\,\mathrm{mol/dm^3}$ is twofold that in helium gas at $1\,\mathrm{mol/dm^3}$. The total macroscopic cross section of a certain nuclide is thus not a physical constant. In order to compare the interaction probabilities of different nuclides, it is useful to divide the macroscopic cross section by the nuclide density to obtain the *microscopic cross section* of the nuclide, which is independent of the material nuclide density and is an intrinsic property of the nuclide.

2.1.2 Microscopic cross sections

The microscopic cross section (denoted with a lowercase sigma σ) is a quantity associated with a certain nuclide (not material) and nuclear reaction type that reflects the likelihood of a neutron to undergo that reaction with that nuclide. The microscopic cross section can be obtained by dividing the macroscopic cross section of the nuclide with the number density of the nuclide for a certain material:

$$\sigma_t^n = \frac{\Sigma_t^n}{N^n} \Leftrightarrow \Sigma_t^n = \sigma_t^n N^n \tag{8}$$

This relation also applies to the individual reaction cross sections, not only to the nuclide total cross section. Therefore the microscopic cross sections can also be divided into the different reaction modes. For example, for ^{1}H it stands similar to Eq. 3 that

$$\sigma_t^{^1\mathrm{H}} = \sigma_\mathrm{s}^{^1\mathrm{H}} + \sigma_\mathrm{c}^{^1\mathrm{H}}. \tag{9}$$

The unit of microscopic cross sections is that of area, but due to the small values of the microscopic cross sections the unit barn (b) is typically used:

$$[\sigma] = 1\,\mathrm{b} = 1 \times 10^{-24}\,\mathrm{cm}^2. \tag{10}$$

2.1.3 Energy dependence of cross sections

The microscopic cross sections, and by extension their macroscopic counterparts, are heavily dependent on the incoming neutron energy. Figure 2 shows the microscopic cross sections of some important reaction modes in nuclear reactors. Due

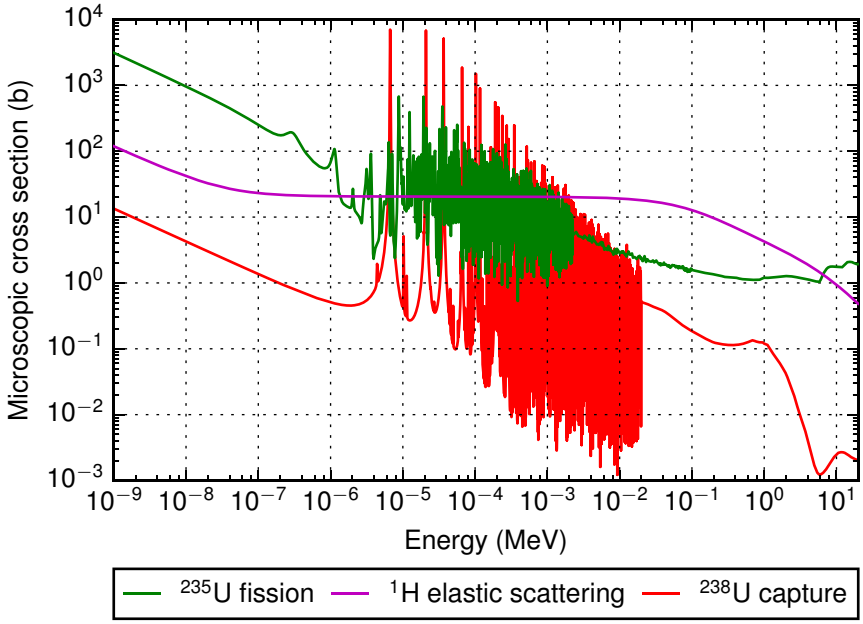

Figure 2. Example of microscopic cross sections of some important reaction modes with two uranium isotopes in nuclear fuel. Data from JEFF-3.1.1 at 300 K temperature.

to the wide variation in both the neutron energy and the interaction probabilities typically seen in reactor applications, it is customary to use logarithmic scales for both axes in cross section plots. Three different energy regions can be established from the plot: The region in the left side of the figure, where all of the three cross sections have a smooth shape, is called the *thermal energy region*. The thermal energy region extends from low energies to approximately 1 eV. At higher energies, we can see high interaction probability peaks in the cross sections at specific energies. At these high probability *resonance energies*, the energy obtained by the compound nucleus produced in the interaction corresponds to the difference of two excitation states of the nucleus, which greatly increases the probability of the interaction resulting in the *resonance peaks* seen in the cross section data. The energy region, where the peaks can be seen in the cross sections, is called the *region of resolved resonances*. At even higher energies, it becomes difficult to resolve the resonance peaks from each other using experimental techniques and only the average smoothed interaction probability can be measured. This high energy region is called the *region of unresolved resonances*.

2.1.4 Temperature dependence of cross sections

As the interaction probability between a neutron and a target nucleus depends on the incoming neutron energy, the interaction probabilities (cross sections) are also temperature dependent. The origin of this temperature dependence is related to the thermal motion of the atoms in the medium that the neutron is travelling in: In a material at a temperature of zero Kelvin, the constituent atoms would experience no thermal motion, i.e. they would be completely stationary targets for any incoming neutrons. In such a case a neutron with a kinetic energy E_0 would experience an interaction probability of $\sigma^{0\,\mathrm{K}}(E_0)$, where $\sigma^{0\,\mathrm{K}}$ now refers to the interaction probability, when the target nucleus is part of a material at zero Kelvin or when the target nucleus is at rest.

At a higher temperature, the constituent atoms of the material are not at rest. Instead, they are subject to random thermal motion based on the Maxwellian distribution at the temperature of the material. Therefore, when a neutron has a kinetic energy of E_0 in the laboratory frame, the energy of the incoming neutron will be slightly different, $E_0 + \Delta E(T)$, in the rest frame of the target nucleus. The additional term $\Delta E(T)$ is a stochastic term that can be positive or negative depending on the velocity and movement direction of the target nuclide. As the interaction probability in the target at rest frame follows the zero Kelvin cross section, it is easy to see that for an interaction between the neutron and a single target nucleus, the interaction probability at an elevated temperature of T will be

$$\sigma^{T}(E_{\mathrm{Lab.}}) = \sigma^{0\,\mathrm{K}}(E_{\mathrm{T\ at\ R}}) = \sigma^{0\,\mathrm{K}}(E_{\mathrm{Lab.}} + \Delta E(T)),$$

where $\Delta E(T)$ is again the stochastic term resulting from the Maxwellian based thermal movement of the target neutron and the lower indices "Lab." and "T at R" indicate energies at the laboratory frame and the target at rest frame, respectively.

This temperature effect is seen at all energies, but it is easiest to understand near the resonance energies of the target nucleus. In Figure 3 this effect is illustrated for a neutron interacting with ^{238}U, when the neutron has the laboratory frame energy corresponding to a certain resonance energy of the target nuclide E_0. If the

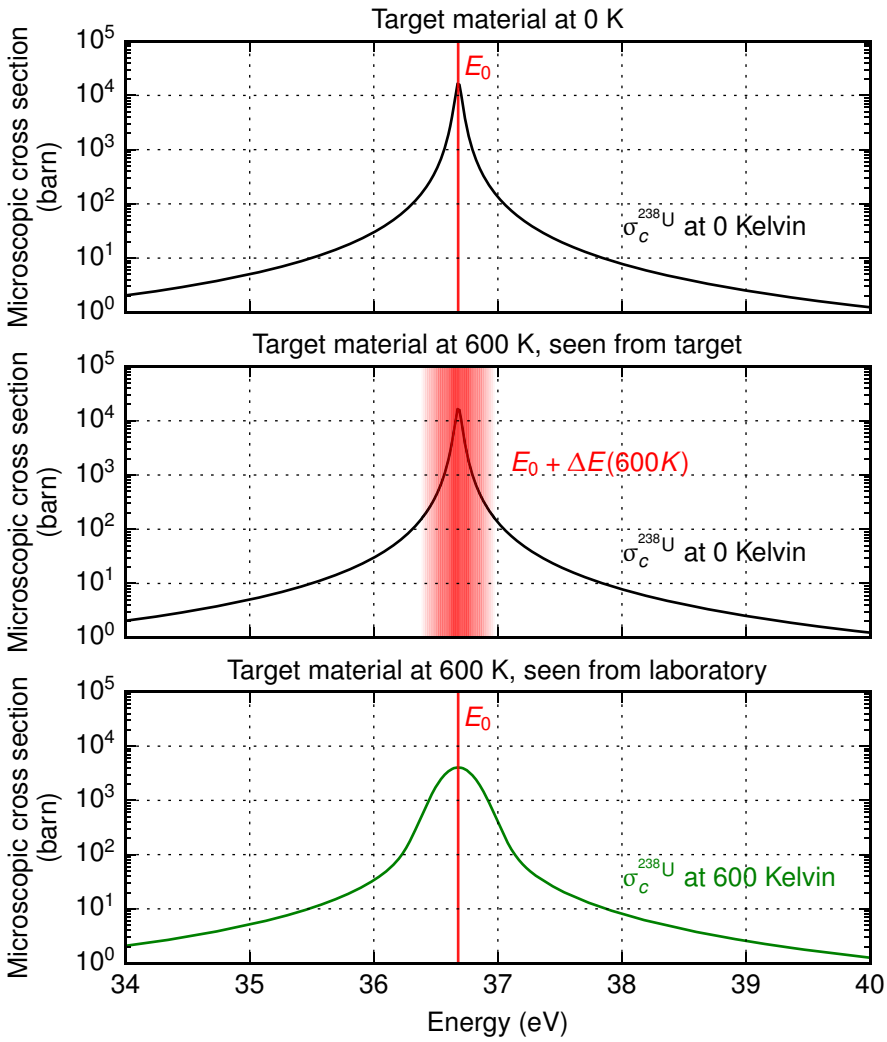

Figure 3. Temperature effect on the microscopic capture cross section σ_c of uranium 238. **Top:** A neutron interacting with uranium 238 at zero Kelvin with energy E_0 that corresponds to the position of the resonance peak has a high probability to undergo radiative capture. **Middle:** If the target nucleus belongs to a material at an elevated temperature (here 600 K), the target nucleus is subject to random thermal motion, which leads to a stochastic modification ΔE(600 K) to the incoming neutron energy in the target at rest frame. **Bottom:** The temperature effect is seen in the laboratory frame as a reduction of the interaction probability at the resonance peak energy and an increase in the interaction probability around the peak energy.

target nuclide is at rest, the interaction probability follows the zero Kelvin cross section for the target nuclide and there is a high probability for the neutron to undergo radiative capture. However, if the target nuclide is in a material at an elevated temperature, the target nuclide is subject to thermal motion following the Maxwellian velocity distribution at the temperature of the material. In the target at rest frame, this is seen as a stochastic modification in the energy of the incoming neutron. The result of this stochastic term is that the energy of the neutron does not necessarily correspond to the resonance energy in the target at rest frame, which, on average, lowers the capture probability. In the laboratory frame this effect of thermal motion of the target is seen simply as a decrease in the capture probability at E_0. At the same time, neutrons that have an energy close to, but not equal to, E_0 in the laboratory frame may have an energy of E_0 in the target at rest frame, which is seen as an increase in the interaction probability at energies around the resonance.

This temperature effect, called the *Doppler broadening* of the resonance peaks, plays a significant role in the control of nuclear reactors and is revisited in Section 4.3.1, when the fuel temperature feedback in thermal reactors is discussed.

2.2 Neutron flux

The objective of reactor physics calculations is to calculate derived results, such as the fission power distribution or atomic transmutation speeds in a certain target, based on the neutron distribution in a nuclear reactor or some other neutronically relevant system. In order to provide the derived quantities, the neutron distribution in the system must first be obtained. Although the energy-dependent neutron density $n(E)$ (neutrons per cm^3) might seem to be a straightforward quantity with which to measure the neutron distribution, the scalar neutron flux

$$\phi(E) = n(E)v(E) \tag{11}$$

is typically a more useful quantity. This is due to the fact that the neutron distribution cannot be measured directly. Rather, reaction rates (reactions per second) or reaction rates integrated over time (total reactions after irradiation of time T) must be measured, and the mathematical expressions for neutron-induced reaction rates contain the product of neutron density $n(E)$ and the neutron speed $v(E)$: The macroscopic cross sections for different reactions give the probability for a neutron with a certain energy to interact on an infinitesimal track-length (Eq. 1). Equation 1 can be rewritten to give the interaction probability during an infinitesimal time increment:

$$\frac{dP}{dt} = \Sigma_t \frac{ds}{dt} = \Sigma_t v, \tag{12}$$

where $v = \frac{ds}{dt}$ is simply the neutron speed. If we now have a constant neutron density of $n(E)$ neutrons per unit volume at energy E moving with a speed $v(E)$ in a material with a material total macroscopic cross section of $\Sigma_t(E)$, we have a reaction rate density of

$$\dot{r}_t = n(E)\frac{dP(E)}{dt} = n(E)\Sigma_t(E)v(E) = \Sigma_t(E)\phi(E) \tag{13}$$

reactions per unit volume per unit time. Physical instruments can only measure reaction rates in a finite volume caused by neutrons at a finite energy range, which

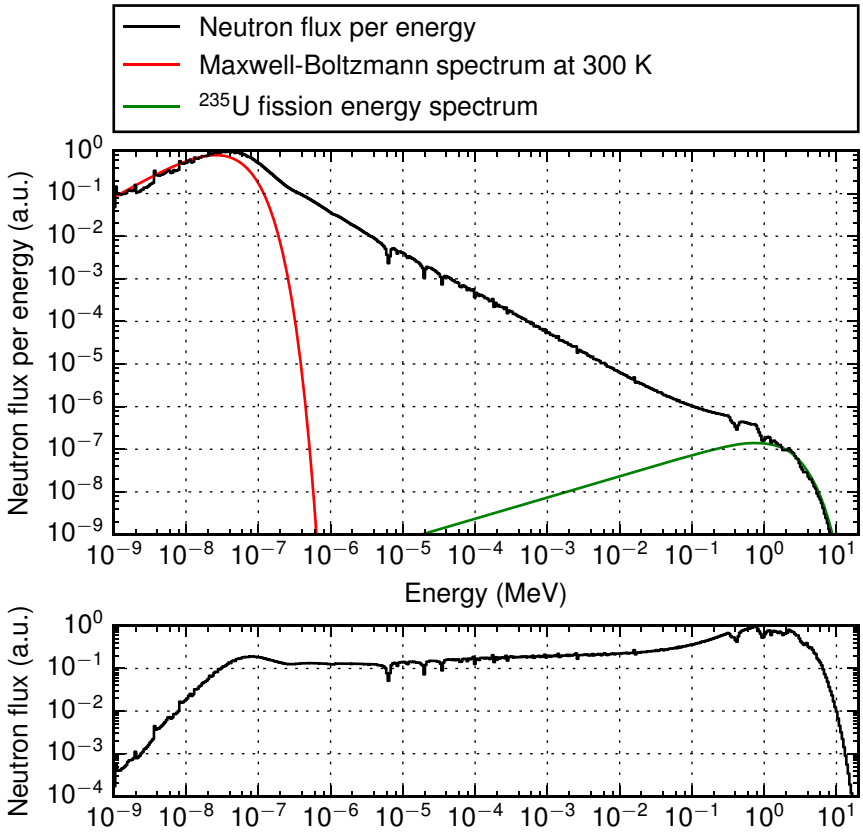

Figure 4. Top: The neutron flux energy spectrum in an LWR-like system shows the typical spectrum shape for thermal reactors. Maxwell-Boltzmann distribution at the moderator temperature is plotted in red, whereas the fission spectrum of ^{235}U is plotted in green. The tallied flux spectrum is normalized to a maximum of 1.0 and the other plotted spectra have been manually scaled to fit the tails of the tallied distribution. **Bottom:** The flux spectrum in the top figure integrated over 500 intervals of equal logarithmic energy width.

can be expressed as a double integral

$$\dot{R}_t = \int_V \int_E \Sigma_t(E)\phi(E)\mathrm{d}E\mathrm{d}V. \tag{14}$$

The previous expression is the total number of all reactions, but typically a specific reaction r of a specific nuclide n is measured

$$\dot{R}_r = \int_V \int_E \Sigma_r^n(E)\phi(E)\mathrm{d}E\mathrm{d}V. \tag{15}$$

Figure 4 shows the scalar flux as a function of energy in a thermal reactor geometry system. The neutron flux was tallied in 500 energy bins with equal logarithmic width using Serpent 2.1.27. For the top figure, the values of each bin were divided by the energy width of the bin while for the bottom figure the values were plotted undivided. Both representations have their merits and are commonly used. The shape of the flux energy spectrum in this figure is typical for thermal reactors. The physical background of the shape of the neutron energy spectrum in thermal systems is discussed in more detail in Section 4.

2.3 Interaction types

Free neutrons can interact with matter through various different interaction types (also referred to as reaction types or reaction modes). This section describes the basics of three interaction types: Scattering reactions, capture reactions and neutron-induced fission reactions. The latter two can be classified as absorption reactions, in which the incident neutron is consumed in the reaction, whereas in scattering reactions the neutron is not consumed, but its energy and direction of movement are altered.

Based on whether the neutron enters the target nucleus or not, the reaction modes can be divided into *potential scattering* and various *compound nucleus reactions*. In the former reaction type, the neutron and the nucleus interact through elastic scattering without the absorption of the neutron into the nucleus, whereas in the latter reaction type the neutron is absorbed into the nucleus, forming a compound nucleus at an excited energy state, which will then decay in one of various ways resulting in one of several different reaction types.

2.3.1 Scattering reactions

Scattering reactions are simple collisions between the neutron and the target nucleus. By definition, at least a single neutron is emitted in the scattering reaction. Based on the scattering kinematics, neutron scattering is further divided into *elastic* and *inelastic* scattering. A third class of reactions, namely (n,xn) reactions, is also introduced here as a group of scattering reactions, although they could be considered to be a reaction type of their own.

Potential scattering is always an elastic scattering reaction, i.e. the initial kinetic energy of the neutron and the atomic nucleus is divided between the neutron and the nucleus. The other possible scattering reactions are elastic compound scattering, inelastic (compound) scattering and (compound) (n,xn) reactions. In elastic compound scattering, the nucleus absorbs the neutron, producing a compound nucleus,

which then sheds all of the gained energy by emitting a single neutron and returning to its initial energy state. A single neutron is also emitted in inelastic scattering, but the target nucleus remains at an excited state. In (n,xn) reactions some additional particles are emitted alongside the outgoing neutron. The x in the (n,xn) represents these additional particles and the group of (n,xn) reactions can be divided into multiple reaction types such as (n,2n) and (n,3n), etc., in which multiple neutrons are emitted from the compound nucleus or charged particle reactions such as (n,pn) or (n,αn), in which a proton or an alpha-particle, respectively, is emitted in addition to the neutron.

Inelastic scattering reactions are *threshold reactions*, which means that they have a minimum energy (*threshold energy*) that will be required from the neutron to induce the reaction. The threshold energies of inelastic scattering typically start from tens of kiloelectronvolts and depend on the energy required to excite the compound nucleus. Elastic scattering reactions, on the other hand, are also common at low energies. The (n,xn) reactions are also threshold reactions as energy is required to dislodge additional particles from the target nucleus.

2.3.2 Capture

Capture reactions are a group of compound nucleus reactions, in which the incident neutron is absorbed by the target nucleus in the process. The excited state of the compound nucleus decays through the emission of a charged particle or a photon, leaving the incident neutron as a part of the target nucleus. Based on the exiting particle(s), the capture reactions can be approximately divided into radiative capture (n,γ), where a photon is emitted, and charged particle reactions such as (n,p) and (n,α), in which a proton and an alpha particle are emitted, respectively.

The capture cross sections of several important nuclides are plotted in Fig. 5. In nuclear reactors, the capture of neutrons by different nuclides serves multiple roles: Many neutrons are lost to radiative capture by ^{238}U during the slowing down of the neutrons in thermal reactors. The light hydrogen (^{1}H) in LWRs also captures some neutrons in the coolant/moderator, leading to a need to isotope-enrich the uranium used in the fuel with respect to the fissile ^{235}U isotope. Another approach to the capture by ^{1}H is to use heavy water (D_2O) as the neutron moderator due to the much lower neutron capture probability by deuterium (^{2}H). Nuclides with a large neutron capture cross section are also used intentionally to control the reactivity of the reactor in control elements (silver-indium-cadmium alloy, boron carbide and borated steel), as burnable absorbers co-mixed with the fuel (gadolinium) or as soluble absorbers mixed with the moderator (boric acid) or in burnable fixed control elements (borosilicate glass).

It should be noted that whereas the radiative capture of neutrons by ^{238}U reduces the number of neutrons able to induce fission reactions, it also leads to the production of ^{239}Pu via the following reaction:

$$ {}^{1}_{0}\mathrm{n} + {}^{238}_{92}\mathrm{U} \rightarrow [{}^{239}_{92}\mathrm{U}^{*}] \rightarrow {}^{239}_{92}\mathrm{U} + \gamma $$

$$ {}^{239}_{92}\mathrm{U} \xrightarrow[23.45\,\mathrm{min}]{\beta^-} {}^{239}_{93}\mathrm{Np} \xrightarrow[2.356\,\mathrm{d}]{\beta^-} {}^{239}_{94}\mathrm{Pu} $$

Plutonium-239 is an important fissile nuclide, and a significant amount of the energy production in the later parts of fuel life is due to ^{239}Pu fissions.

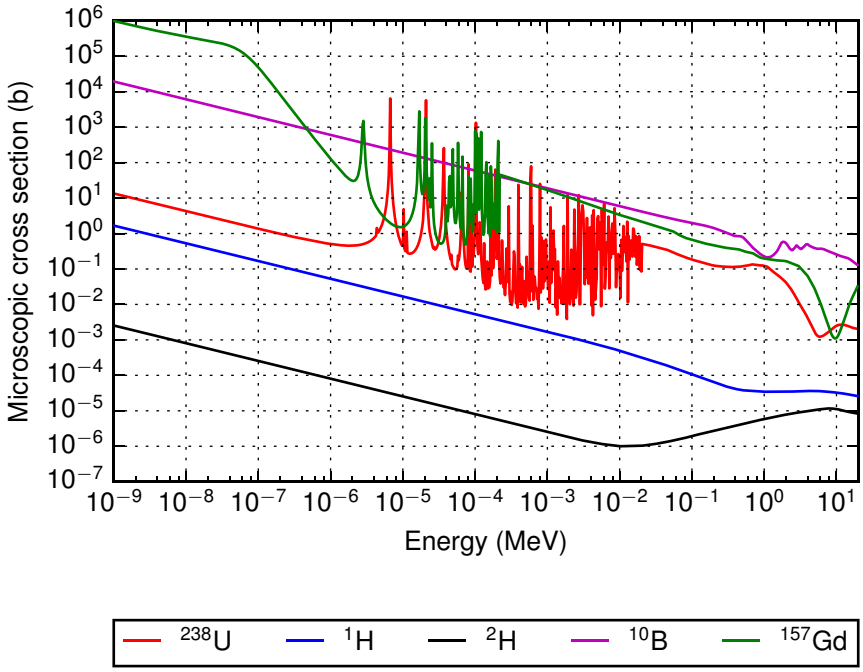

Figure 5. Microscopic capture cross sections of several important nuclides from the point of view of reactor physics. The straight $1/\sqrt{E}$ base shape of the curves is broken by resonances. The cross sections of heavier nuclides exhibit more resonances due to a greater number of possible excitation states for the compound nucleus formed in the neutron absorption.

Table 1. Quantities related to the fission of some interesting fissile and fertile nuclides used in nuclear fuel at two incident neutron energies. Data from JEFF-3.1.1.

		Fissions per absorption σ_f/σ_a		Fission energy release Q (MeV)		Fission neutron release $\bar{\nu}$	
Incident energy:		0.3 eV	3 MeV	0.3 eV	3 MeV	0.3 eV	3 MeV
^{232}Th	(fertile)	0.00	0.82	200	202	2.17	2.29
^{233}U	(fissile)	0.92	0.99	198	198	2.49	2.83
^{235}U	(fissile)	0.81	0.98	202	203	2.44	2.77
^{238}U	(fertile)	0.00	0.98	209	209	2.41	2.79
^{239}Pu	(fissile)	0.60	0.99	206	206	2.85	3.30
^{241}Pu	(fissile)	0.66	0.98	210	210	2.93	3.38

2.3.3 Neutron-induced fission

In neutron-induced fission reactions, the compound nucleus formed by the neutron absorption has sufficient energy to split into typically two smaller nuclei. In the fission reaction of heavy elements, a significant amount of binding energy is released (see Table 1). This released energy is the basis of power production in nuclear fission reactors.

The fissions also release free neutrons at a relatively high energy (in the MeV range). These instantaneously released fission neutrons are called *prompt neutrons* due to their prompt emission. The produced fission fragments have a high neutron-to-proton ratio for their mass number and many of them decay to a more favorable neutron-proton configuration via beta decay. Some of the beta decay events for certain fission fragments can release sufficient energy to knock out a neutron from the atom nucleus. These neutrons, emitted due to the beta-decay of the fission fragments on a broad timescale of milliseconds to minutes after the fission event, are called *delayed neutrons* due to their delayed emission. Although the fraction of delayed neutrons of all neutrons released due to a fission reaction is small, they are very important for the control of the nuclear reactor due to their delayed emission. There is a large number of potential delayed neutron precursor nuclides ([11] lists over 150 nuclides in the fission product range that models predict to emit delayed neutrons) and they are typically grouped to a small number of groups based on their decay constants in the evaluated nuclear data libraries such as ENDF/B and JEFF.

In typical nuclear fuel nuclides, the number of neutrons released in a fission reaction and the subsequent radioactive decay of the fission products is significantly greater than one, the number of neutrons lost in the fission reaction. Table 1 also shows the average number of neutrons produced due to the fission of several fuel isotopes at two different incident neutron energies. At thermal energies, approximately 1.4 – 1.9 neutrons are gained in addition to offsetting the single neutron lost in the fission. The number of produced prompt fission neutrons increases as a function of incident neutron energy due to the addition of energy to the compound nucleus formed by the neutron absorption. This release of fission neutrons makes it possible to produce a stable neutron chain reaction, which is essential for the steady

state operation of fission reactors.

All nuclides with an atomic number higher than 90 can be made to fission if the kinetic energy of the incident neutron is sufficiently high. Although all nuclides that can be made to fission are typically called *fissionable*, there is a subset of fissionable nuclides that fission with a high probability regardless of incident neutron energy. These *fissile* nuclides are important for producing a fission chain reaction in nuclear reactors. This can be seen in Table 1: The probability of fission by absorption of 0.3 eV neutrons is very low for ^{232}Th and ^{238}U. Based on this, these two nuclides are not fissile. However, the radiative capture of neutrons by ^{232}Th will lead to the production of fissile ^{233}U and the radiative capture by ^{238}U will produce fissile ^{239}Pu. Nuclides that can be transmuted to fissile nuclides through neutron capture are called *fertile*.

To complete the nomenclature concerning nuclides that can fission, it should be noted that some nuclides, such as ^{240}Pu, are not fissile, i.e. they cannot reliably be fissioned with low energy neutrons, but can support a fast neutron chain reaction. Kelly and Clayton proposed *fissible* as a separate term for nuclides capable of supporting a neutron chain reaction with high-energy neutrons ($>\approx$1 MeV) but not with neutrons at the thermal energy range [12].

2.4 Multiplication factor and reactivity

Balancing the neutron production from fission reactions with the neutron loss to capture reactions and neutron leakage is the basis of neutron-economical design of nuclear reactors: Some of the neutrons released in fission reactions leak out of the reactor or are lost in capture reactions with the materials in the reaction. Other neutrons manage to induce new fission reactions, producing the next generation of fission neutrons. The average number of fission neutrons produced by a single fission neutron in a system is called the *effective multiplication factor* of the system and denoted with $k_{\text{eff.}}$. The effective multiplication factor is a useful quantity, as it is easy to see that a multiplication factor less than unity corresponds to a diminishing chain reaction (the neutron population decreases, the system is *sub-critical*) and a multiplication factor greater than unity corresponds to a growing chain reaction (the neutron population increases, the system is *supercritical*). A multiplication factor of exactly 1 corresponds to a stable chain reaction (the neutron population remains constant, the system is *critical*).

As the multiplication factor in reactor applications is typically close to unity (the power level of the reactor is stable or changing only slowly), it is often easier to work with the *reactivity* of the system

$$\rho = \frac{k_{\text{eff.}} - 1}{k_{\text{eff.}}}, \tag{16}$$

which is typically given in pcm (per cent mille)

$$1\,\text{pcm} = 1 \times 10^{-5} = 0.001\,\%. \tag{17}$$

Based on the multiplication factor it is easy to deduce that the reactivity of a critical system is zero. Negative reactivities correspond to a sub-critical system, whereas positive reactivities correspond to a super-critical system.

3. Monte Carlo neutron tracking

Whereas deterministic neutron transport solvers are based on solving the Boltzmann transport equation for neutrons using several simplifications[2] that are required to obtain a solution, the Monte Carlo approach completely bypasses the transport equation. Instead of modeling the neutron flux as a distributed quantity, individual neutron histories are modeled as a random walk process and the behavior of the neutron population at large is gleaned through statistical estimates obtained for a large number of individual neutron histories.

3.1 Neutron transport as a random walk

The Monte Carlo methods approach the neutron transport problem by simulating the interactions of individual neutrons with high detail from their birth to the eventual absorption or leakage of the neutron. The advantage of the Monte Carlo method is that, even in extremely complex systems, the computational process for modeling the individual neutron histories can be divided into a series of relatively simple steps:

0. Start with a source neutron with a certain position $\vec{r}_0$ and velocity $\vec{v}_0 = v_0\hat{\Omega}_0$.
1. Sample track-length to the next interaction: s.
2. Move the neutron to the interaction site.
3. Sample the interaction that the neutron will experience.
4. Model the reaction
5. If the reaction was an absorption, model the next history. Otherwise continue from 1 with the current neutron position and velocity.

Statistical estimates for various variables such as reaction rates, neutron production or loss rates, neutron kinetic parameters and many others can be collected during the simulation.

The physics enters the random walk through modeling the interactions based on the best possible experimental and theoretical models and basing the random sampling of neutron track-lengths and interactions on physical probabilities — the macroscopic and microscopic cross sections. The following sections will describe the individual parts of the random walk in greater depth.

3.2 Sampling track-lengths

The track-length from one interaction to the next in an infinite homogeneous medium follows the probability density function given in Eq. 5 and can be sampled using the cumulative inverse sampling procedure, in which first the cumulative distribution function is calculated

$$P_{\mathrm{CDF}}(E,s) = \int_0^s \mathbb{P}(E,s)\mathrm{d}s = \int_0^s \Sigma_t(E)e^{-s\Sigma_t(E)}\mathrm{d}s = 1 - e^{-s\Sigma_t(E)}, \tag{18}$$

[2] Typical simplifications are spatial discretization and homogenization, energy discretization and condensation, angular discretization of neutron travel directions and time discretization.

whereafter the inverse of the cumulative distribution function is obtained. Denoting the value of the CDF with ξ, we can derive

$$\begin{aligned}
\xi &= 1 - e^{-s(E,\xi)\Sigma_t(E)} \\
\log[1-\xi] &= \log\left[e^{-s(E,\xi)\Sigma_t(E)}\right] \\
\log[1-\xi] &= -s(E,\xi)\Sigma_t(E) \\
s(E,\xi) &= -\frac{\log[1-\xi]}{\Sigma_t(E)} \\
s(E,\xi) &= -\frac{\log[\chi]}{\Sigma_t(E)}.
\end{aligned} \tag{19}$$

Now sampling random numbers from the unit interval $\chi \in [0,1)$ we can sample track-lengths that follow the PDF in Eq. 5. It is important to note that the derivation of the PDF assumes an infinite homogeneous medium, in which the macroscopic total cross section is independent of location. In reality, Σ_t also depends on the spatial location and will be written as $\Sigma_t(E,\vec{r})$. This means that situations, in which the sampled track length extends over a material boundary require special consideration. There are two approaches for the non-constant Σ_t which are briefly described here.

In the surface tracking algorithm, also sometimes referred to as ray-tracing [13], the track-lengths that extend out of the initial material region are stopped at the first material boundary and a new track-length is then sampled in the upcoming material.

In the Woodcock delta tracking algorithm [14], rejection sampling is used instead. The derivation of the Woodcock delta tracking algorithm may be conceptually easiest to perform via the introduction of virtual interactions[3]: The virtual interactions that have an associated macroscopic cross section of $\Sigma_{\text{virt.}}$ are interactions that do not change the neutron's movement direction or speed in any way. The idea is then to first find out the maximum material total cross section at each incoming neutron energy, also called the *majorant cross section*

$$\Sigma_{\text{maj.},t}(E) = \max \Sigma_t(E,\vec{r}), \tag{20}$$

where the maximum is taken over the whole geometry. The next step is to "pad" each material total cross section with a different amount of the virtual cross section so that the modified material total cross section is the same throughout the geometry, e.g.

$$\Sigma_t^*(E,\vec{r}) = \Sigma_{i,t}(E,\vec{r}) + \Sigma_{i,\text{virt.}}(E,\vec{r}) = \Sigma_{\text{maj.},t}(E), \tag{21}$$

where $\Sigma_t^*(E,\vec{r})$ is the padded macroscopic cross section at $\vec{r}$ and $\Sigma_{i,\text{virt.}}(E,\vec{r})$ is the virtual cross section added to the total cross section at $\vec{r}$. After the addition of the virtual cross sections the whole geometry has the same cross section

$$\Sigma_t^*(E,\vec{r}) = \Sigma_{\text{maj.},t}(E), \qquad \text{for all } \vec{r}, \tag{22}$$

which is independent of the spatial coordinates and can be used to sample the track-lengths. The track-lengths sampled using the majorant cross section will be, on average, shorter than if the local material total cross section would be used. However, the physicality of the simulation is preserved by rejecting a fraction of

[3] The other possibility would be through the concept of rejection sampling.

the sampled interaction points as virtual interactions (see Section 3.4) that do not affect the movement of the neutron in any way. This will conserve the track-length distribution between two non-virtual interactions [15].

3.3 Moving the neutron

In order to move the neutron to the sampled interaction site, only the neutron position has to be updated. If the initial position and direction of the neutron were $\vec{r}_0$ and $\hat{\Omega}_0$, respectively, and the sampled track-length was s, the new neutron position would simply be

$$\vec{r}_1 = \vec{r}_0 + s\hat{\Omega}_0. \tag{23}$$

In time-dependent simulations, the neutron time can also be updated. If the time at the beginning of the track-length was t_0, the new time is simply the previous time incremented with the track-length divided by the neutron speed[4]:

$$t_1 = t_0 + \frac{s}{v_0}. \tag{24}$$

3.4 Interaction sampling

When the neutron has been moved to its interaction site $\vec{r}_1$ the interaction type must be sampled. If the track-length was sampled using delta tracking, it is first necessary to establish whether the interaction will only be a virtual reaction. The probability of a virtual reaction is simply the ratio of the virtual cross section to the padded total cross section

$$P_{\text{virt.}} = \frac{\Sigma_{\text{virt.}}(E, \vec{r}_1)}{\Sigma_t^*(E, \vec{r}_1)} = \frac{\Sigma_{\text{virt.}}(E, \vec{r}_1)}{\Sigma_{\text{maj.},t}(E)}. \tag{25}$$

If a virtual reaction is sampled, the new track-length can be sampled immediately.

If the reaction was not virtual or the track-length was sampled using surface tracking, the target nuclide and reaction mode can be sampled. It should be noted that the macroscopic total cross section is a sum of the macroscopic total cross sections of the different nuclides in the material (Eq. 2) and the cross section of each nuclide is a sum of the individual reaction mode cross sections for that nuclide (Eq. 3). If an interaction has been sampled to occur, the probability for the interaction to be with nuclide n with reaction type r is then the reaction r macroscopic total cross section for nuclide n divided by the material macroscopic total cross section:

$$P(\text{target} = n, \text{reaction} = r, E) = \frac{\Sigma_r^n(E, \vec{r})}{\Sigma_t(E, \vec{r})}. \tag{26}$$

The target and reaction can be sampled simply by sampling a random number from the unit interval ξ and then summing the individual reaction cross sections divided by the macroscopic material total cross section until the sum exceeds ξ (see Algorithm 1).

[4] To be precise, relativistic effects generally have to be accounted for when modeling fast neutrons ($E \approx 10$ MeV and higher).

Algorithm 1. Algorithm for sampling target nuclide and interaction type in Monte Carlo neutron tracking.

```
0 :  ξ = rand(0, 1)
0 :  a = 0
1 :  for n in 0, 1, ... , N_n:
2 :      for r in 0, 1, ... , N_{r,n}:
3 :          a = a + Σ_r^n(E)/Σ_t(E)
4 :          if a > ξ: break
5 :      end for
6 :      if a > ξ: break
7 :  end for
8 :  Reaction target nuclide n reaction type r.
```

3.5 Modeling interactions

After the interaction has been sampled, the reaction is modeled based on the interaction type. The interested reader is directed to the physics section of the OpenMC Monte Carlo code documentation [16], but some simplified examples of interaction modeling in the context of the random walk are given here:

- Scattering reactions: Update neutron energy and direction based on elastic or inelastic scattering kinematics[5].
- Capture reactions: Terminate the neutron track.
- Fission reactions: Terminate the neutron track and sample a number of fission neutrons. For each fission neutron sample, whether the neutron is prompt or delayed. For delayed neutrons sample the emission time based on the delayed neutron group structure of the fissioning isotope obtained from the nuclear data library. Finally, sample the emission direction and emission energy for each produced neutron.

Sampling in the interaction modeling is performed either based on analytic descriptions of reaction kinematics (e.g. scattering reactions) or on tabulated data (e.g. delayed neutron fractions and fission spectra).

3.6 Tallying results

The results obtained from a Monte Carlo simulation are statistical estimates. There are several ways to calculate these estimates: The simplest way is to use *analog estimators*, which simply means that each time an event of interest is sampled, a score is added to a tally. The final score of the tally at the end of the simulation then represents the probability of that event of interest. For example, we could tally the number of interactions that occur with ^{1}H as the target nucleus simply by adding 1

[5] Separate treatments can be applied to high and low energy regions and for bound scatterers.

to a tally each time ^{1}H is sampled as the target nuclide in the interaction sampling. The probability of adding 1 to the tally would then simply be

$$P(\text{add 1}) = P(\text{target} = {}^1\text{H}) = \frac{\Sigma_t^{^1\text{H}}}{\Sigma_t}. \tag{27}$$

The disadvantage of analog estimators is the fact that the tally is only incremented when the event of interest is actually sampled. If the probability of the event is low, there might only be a few scores in the tally, which makes the uncertainty associated with the result high. A better way would then be to use an *implicit estimator*, for example the *collision estimator*, in which instead of adding 1 to the tally with the probability of the event, we add the probability of the event to the tally with a probability of 1. In the hydrogen example, we would simply add

$$\frac{\Sigma_t^{^1\text{H}}}{\Sigma_t} \tag{28}$$

to the tally at each interaction, whether or not the sampled target nuclide is actually ^{1}H. The use of implicit estimators results in adding smaller values to the tally more frequently, and via an increased number of samples better statistics are obtained. The alternative to the collision estimator is to use the *track-length estimator*, which will add the probability of the event of interest over the previous track-length s rather than at the current collision:

$$\frac{\Sigma_t^{^1\text{H}}}{\Sigma_t} s. \tag{29}$$

If the track-length extends over multiple material regions, as can occur with the use of delta-tracking, the cross sections in Eq. 29 are not constant over the track-length. In such cases, the track-length must be divided into multiple segments s_i, with each segment lying in a single material region with constant cross section $\Sigma_{r,i}^n$. The track-length estimate can then be summed up through the whole track-length with

$$\sum_i \frac{\Sigma_{t,i}^{^1\text{H}}}{\Sigma_{t,i}} s_i. \tag{30}$$

The track-length estimator makes it easy to obtain statistical estimates in materials that have a small Σ_t and thus a low interaction probability. The collision estimator is scored each time an interaction point is sampled and by default interaction points are rarely sampled into materials with a low Σ_t. The efficiency of the collision estimator in low Σ_t materials can be enhanced by increasing the small material total cross sections via the use of the virtual cross section $\Sigma_{\text{virt.}}$, as the collision estimator can be scored even if the interaction ends up being a virtual one.

4. Operation of thermal reactors

As described in the previous sections, the operation of nuclear reactors is based on the chain reaction of fissions caused by neutrons. The fission neutrons are born with a relatively high kinetic energy (see green curve in Fig. 4). There are two main approaches to reactor design, based on how these fission neutrons are led to induce the next generation of fissions. *Fast reactors* are based on fissions induced by the high-energy (fast) fission neutrons with the least number of other interactions between the birth of the neutrons and the consumption of the neutrons in a new fission event. *Thermal reactors* are based on slowing the high-energy neutrons to low kinetic energies via collisions with the atoms of a *moderator* material, before allowing the neutrons to induce a new fission.

Although multi-physics problems exist both in fast and thermal systems, the applications in this thesis were from thermal systems[6]. For this reason, only the thermal neutron chain reaction and the main temperature feedback mechanisms in a thermal reactor are described in the following.

4.1 Thermal neutron chain reaction

The advantage of slowing down the fission neutrons to thermal energies can be seen in Fig. 6. In order to have a non-decreasing chain reaction, each absorption of a neutron to the fuel must, on average, produce at least one neutron. With the enrichment of the fuel being at or below 5 wt.% this is only possible for neutrons at energies lower than 2–3 eV or higher than 1 MeV. However, as the top part of the figure shows, the absorption probability at high energies is rather low, of the order of 1×10^{-2}/cm. This translates to a mean track-length of 100 cm before an absorption reaction occurs. The probability for the neutron to scatter from a fuel or coolant nuclide before being absorbed to the fuel is high, and each scattering reaction will make the neutron lose energy and move it farther from the high-energy region.

The thermal reactor design embraces the energy loss in scatterings and aims to slow the neutrons down to thermal energies around 0.025 eV, at which both the number of neutrons produced per absorption in the fuel and the absorption probability are high. The potential downside of slowing the neutrons down stems from the fact that should the neutrons return to the fuel material in the resonance energy range, there is a high probability of their being lost in resonance absorption without the production of new fission neutrons.

The thermal neutron chain reaction then relies on ensuring first that a large percentage of the fission neutrons reach the moderator material, and second that the neutrons shed their kinetic energy by scattering in the moderator quickly, with a low probability of returning to the fuel at intermediate energies. The energy loss of the neutrons in scattering reactions is inversely proportional to the mass of the target nucleus. The maximum energy loss (slowing down) is thus achieved in moderator materials consisting of light elements. For this reason, some of the most popular moderator materials include light water (H_2O), heavy water (D_2O) and graphite (C).

[6] The multi-physics capabilities developed in this thesis are applicable to both thermal and fast systems.

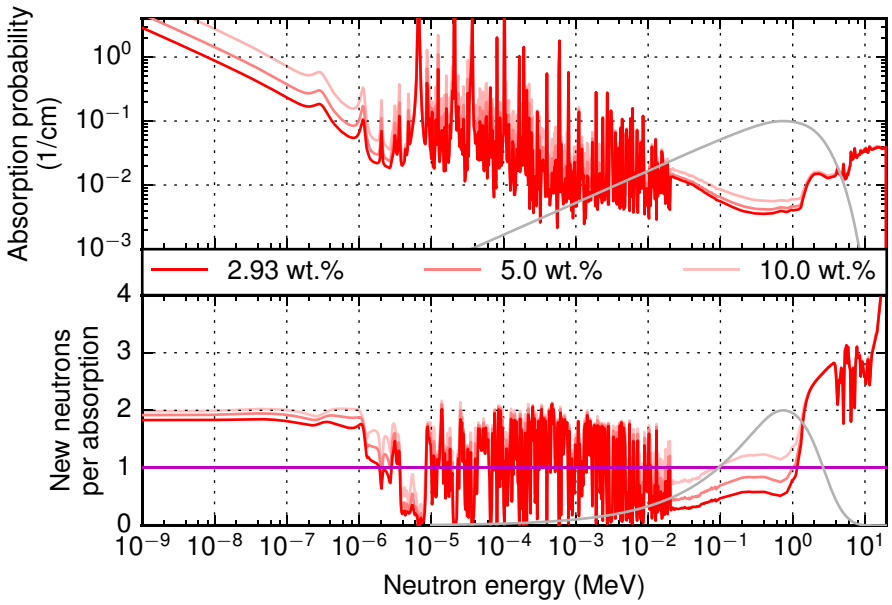

Figure 6. Energy-dependent neutron interaction properties of LEU fuel at three different enrichments. Energy spectrum of fission neutrons is plotted in both figures in grey with arbitrary units. **Top**: The absorption probability per unit distance traveled in fuel. **Bottom**: The average number of neutrons produced by absorption of a single neutron to the fuel.

4.2 Heat transfer in thermal reactors

Figure 7 shows a schematic picture of the different parts of a nuclear reactor relevant for this section. Most of the heat released in the fission reactions is deposited in the fuel material, which is typically contained in long narrow fuel rods (pellets inside a cladding). In the fuel rods the heat conducts through the pellet, the gas gap and the cladding to the cladding outer surface. From the cladding surface the heat is transferred to the coolant. Some of the energy released in the fission reactions is also directly deposited to the coolant, neutron absorbers such as control rods and structural materials by neutrons and photons. The coolant material transfers the heat out of the core and will be either cooled down in heat exchangers providing heat to a secondary coolant circuit (most reactor types), or led directly to a steam turbine (boiling water reactors).

In order to safely operate at constant power there is a simple requirement for the heat balance of the core: The amount of heat produced in the core in unit time must equal the amount of heat transferred out of the core in unit time. Specifically, this can be divided into two important balance requirements:

- The power deposited to the fuel must be equal to the power transferred from

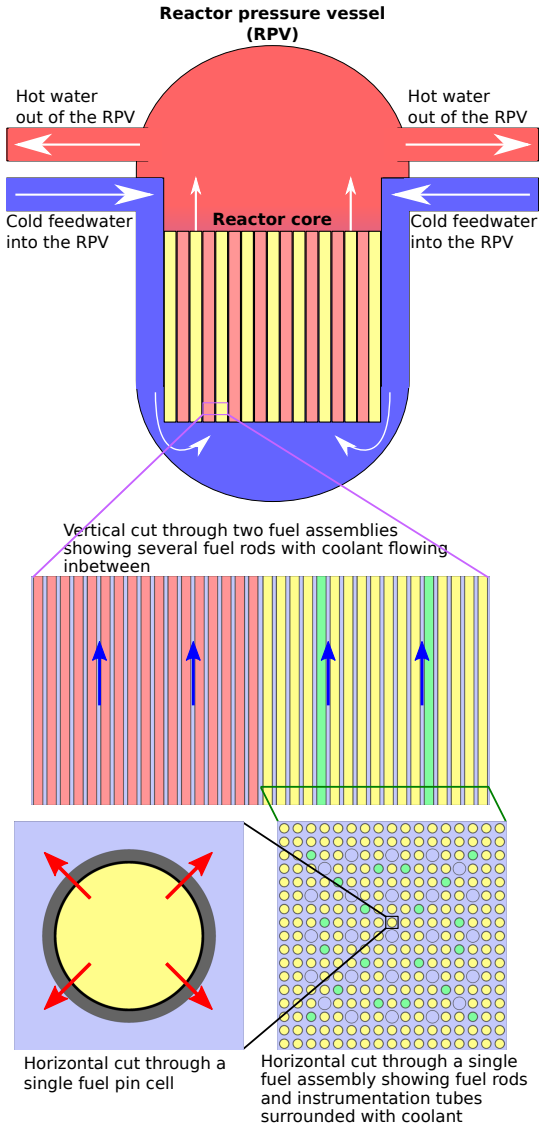

Figure 7. Schematic picture of heat transfer in a light water reactor. The heat deposited in the fuel is transferred horizontally to the cladding surface and coolant (red arrows). The coolant transports the heat by flowing vertically through the core (blue arrows). Cold water enters the reactor core from the bottom and hot water is extracted from the top part of the pressure vessel.

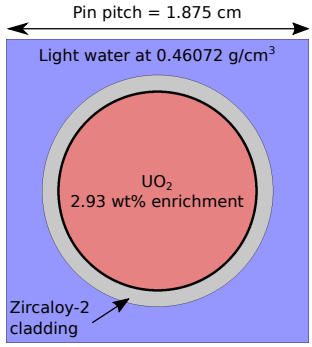

Figure 8. Unit cell of the infinite lattice geometry used to illustrate the thermal feedback effects in an LWR core. Rod and lattice geometry as well as material compositions are from the Peach Bottom 2 benchmark in [17].

the fuel rod to the coolant.

- The power transferred from the fuel rods to the coolant and the power deposited directly to the coolant must be equal to the power transferred out of the core by the coolant.

A failure to fulfil the first requirement will result in an increase in fuel temperature, which, if left uncontrolled, can lead to shattering of the fuel pellet or melting of the fuel. Failure to fulfil the second requirement will lead to an increase in coolant temperature, which can result in reduced heat transfer from fuel rods to the coolant and thus an increase in the fuel temperature.

4.3 The multi-physics coupling in a thermal reactor core

In order to decrease the possibility of sudden adverse increases in the reactor power level, nuclear reactor design makes use of several natural laws to ensure that the power feedback in the reactor is negative in the operating conditions, i.e. that an increase in the power will bring about feedback effects that limit the increase in power. As these feedback effects are based on the physics of the neutron interactions, they are automatic and require no human intervention. The power feedback of a well-designed nuclear reactor is a prime example of passive safety. The three main feedback effects utilized in light water reactor (LWR) design, namely fuel temperature, moderator temperature and moderator density feedback are introduced in the following sections.

Some results tallied from example criticality source (k-eigenvalue) calculations are shown in order to illustrate the different thermal feedback effects in an LWR-like system. The calculation geometry is an infinite 2D lattice of low-enriched uranium fuel rods. The unit cell of the calculation geometry is shown in Fig. 8. The fuel outer radius was 0.605 79 cm, the cladding outer radius was 0.715 01 cm and the cladding thickness was 0.093 98 cm. This simple geometry is infinite both horizontally and axially, which while obviously not realistic, is not very far from the perception of neutrons that are born in the middle of a large LWR core.

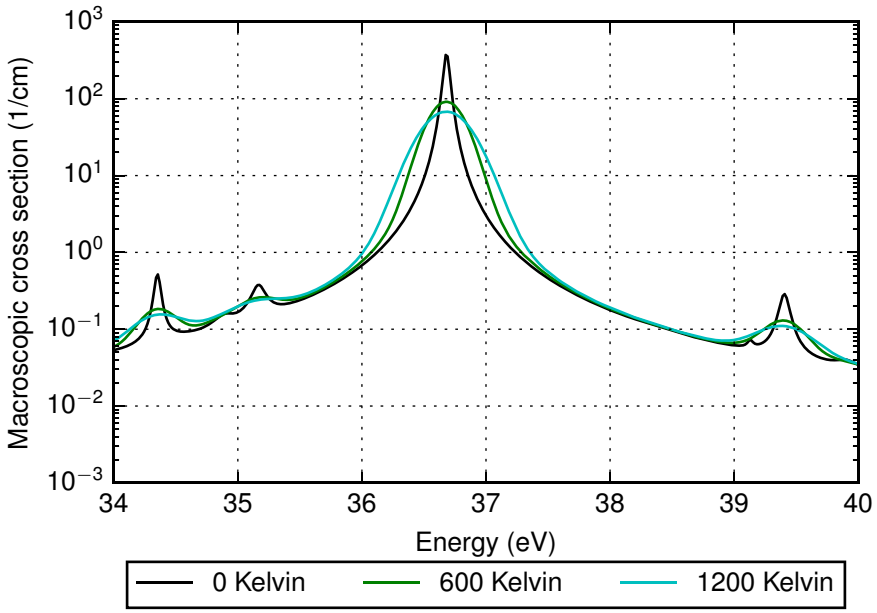

Figure 9. Effect of Doppler broadening on macroscopic capture cross section of low enriched UO_2 fuel at energies close to the ^{238}U resonance at 36.7 eV. Three different fuel temperatures. Data from JEFF-3.1.1.

4.3.1 Fuel temperature feedback

The fuel temperature feedback in LWR reactors is based on the temperature effects on the cross sections of the fuel nuclides, or more specifically, on the Doppler broadening of the resonances in the radiative capture cross section of ^{238}U. An increase in the fission power brings about an increase in the fuel temperature, which affects the neutron interaction probability in the fuel: The probability of neutrons in the resonance energy range being consumed in radiative capture reactions with ^{238}U increases more than the probability of neutrons producing new neutrons in neutron-induced fission reactions. This increases the loss of neutrons in the system and decreases the reactivity. Conversely, a decrease in fuel temperature will decrease the probability of neutrons undergoing radiative capture, which introduces positive reactivity into the system.

Figure 9 shows the Doppler broadening effect on the macroscopic capture cross section of 2.93 wt.% enriched UO_2 fuel with a density of 10.42 g/cm^3 near the 36.7 eV resonance of ^{238}U. The effects of the Doppler broadening are easy to see: The resonance peaks in the cross section become flatter and wider. Figure 10 shows the effect of this Doppler broadening on the neutron flux in the fuel material of the example geometry at the same energy range[7]. For the high resonance, the

[7] For this plot the calculation was normalized to fission power.

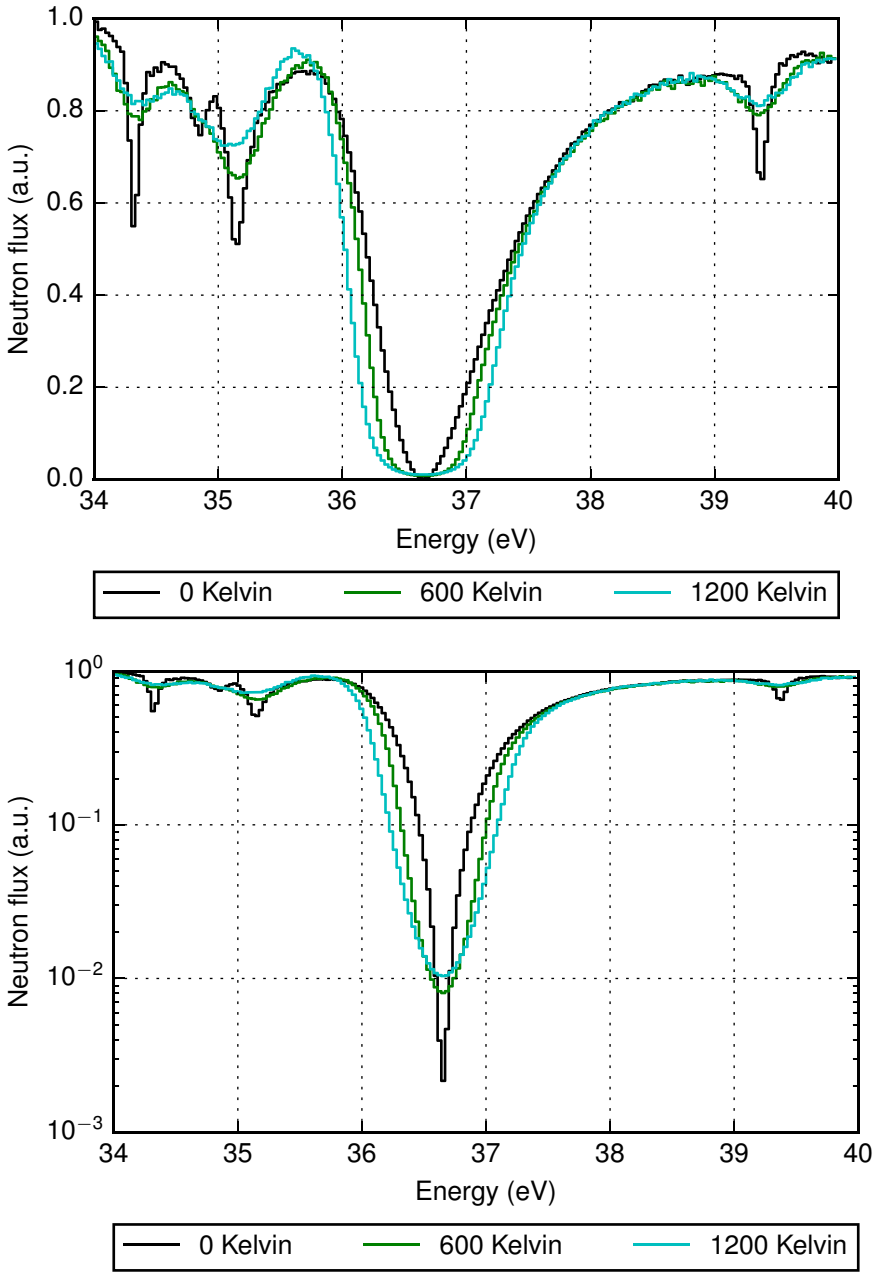

Figure 10. Effect of Doppler broadening on neutron flux in fuel in the example geometry at energies close to the ^{238}U resonance at 36.7 eV. Flux spectrum with three different fuel temperatures calculated with Serpent 2. **Top:** Linear y-axis. **Bottom:** Logarithmic y-axis.

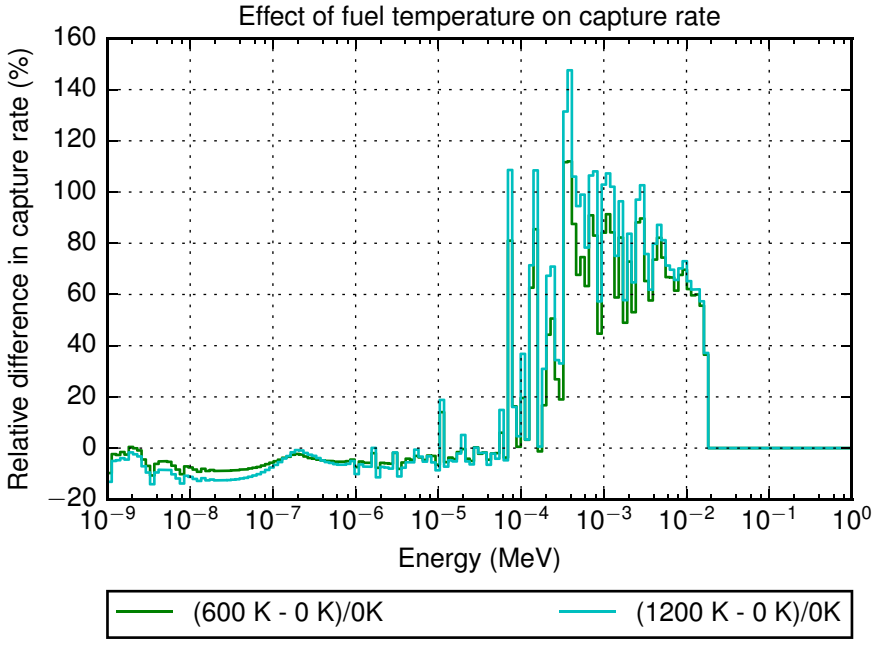

Figure 11. The neutron capture rate in the example geometry was tallied into 200 bins of equal logarithmic width using three different fuel temperatures. This figure shows the relative difference in the neutron capture rate at different energies between the simulations with an elevated fuel temperature and the simulation with a 0 K fuel temperature. Eigenvalue simulation with flux normalization to 1 neutron per second source rate.

flattening of the peaks does not offset the widening of the peak. Neutrons are lost from a wider energy range around the resonance, which increases the total number of neutrons lost to the resonance capture.

An increase in neutron loss in the resonance energy range decreases the number of neutrons that manage to thermalize to the high fission probability thermal energy region and provides a negative reactivity feedback to the system. This is illustrated in Figures 11–13. The flux in these simulations is normalized to a fixed source rate (1 fission neutron per second), which means that the neutron flux at high energies is equal between the simulations. Figure 11 shows the relative difference in the neutron capture rate between simulations with an elevated fuel temperature (600 or 1200 K) and a fuel temperature of 0 K. At the energy range of the unresolved resonances (energies greater than approximately 2×10^{-2} MeV), the capture rate is similar for all fuel temperatures. At the region of resolved resonances, the capture rates are much higher in the systems with elevated fuel temperature, although the differences are smaller at the low energy end of the region. The effect on the flux energy distribution is shown in Figure 12. The increased neutron capture in the

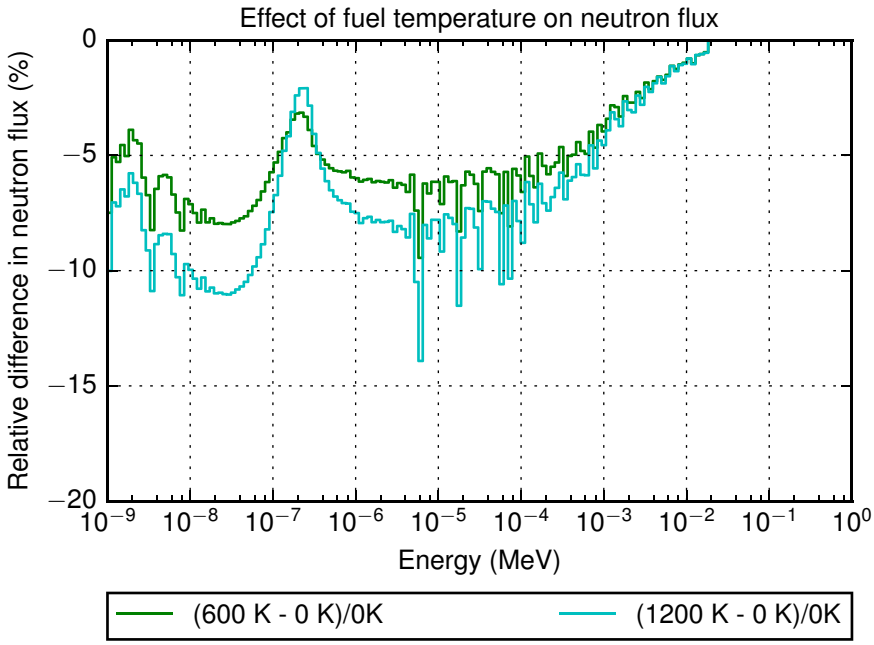

Figure 12. The neutron flux in the example geometry was tallied into 200 bins of equal logarithmic width using three different fuel temperatures. This figure shows the relative difference in the neutron flux at different energies between the simulations with an elevated fuel temperature and the simulation with a 0 K fuel temperature. Eigenvalue simulation with flux normalization to 1 neutron per second source rate.

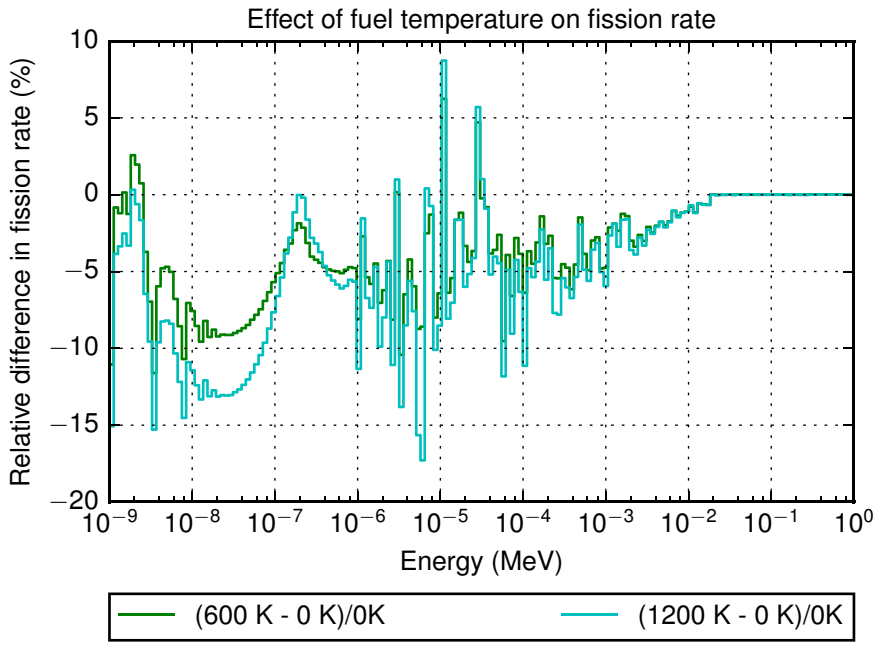

Figure 13. The fission rate in the example geometry was tallied into 200 bins of equal logarithmic width using three different fuel temperatures. This figure shows the relative difference in the fission rateat different energies between the simulations with an elevated fuel temperature and the simulation with a 0 K fuel temperature. Eigenvalue simulation with flux normalization to 1 neutron per second source rate.

Table 2. Tallied capture rate, neutron flux and fission rate in the thermal (< 0.625 eV) and fast (> 0.625 eV) energy ranges in the example geometry using three different fuel temperatures. The flux was normalized to 1 fission neutron per second source rate.

	Capture rate (1/s)		Relative difference compared to 0 K	
	Thermal	Fast	Thermal	Fast
0 K	0.161	0.306	–	–
600 K	0.151	0.345	-6.23 %	12.56 %
1200 K	0.148	0.356	-8.05 %	16.42 %

	Neutron flux ($1/(\mathrm{cm}^2\,\mathrm{s})$)		Relative difference compared to 0 K	
	Thermal	Fast	Thermal	Fast
0 K	7.43	55.9	–	–
600 K	7.01	54.9	-5.58 %	-1.72 %
1200 K	6.92	54.7	-6.79 %	-2.15 %

	Fission rate (1/s)		Relative difference compared to 0 K	
	Thermal	Fast	Thermal	Fast
0 K	0.392	0.143	–	–
600 K	0.366	0.139	-6.42 %	-2.35 %
1200 K	0.359	0.138	-8.43 %	-3.02 %

systems with elevated fuel temperature leads to a steady decrease in the neutron flux at the energy region of resolved resonances. Some low energy effects can be observed around 2×10^{-7} MeV that are explained by the fact that low energy neutrons scattering from fuel at an elevated temperature may gain energy, whereas low energy neutrons neutrons scattering from 0 K fuel material will always lose energy (see the next section for details). The effect on fission rates is shown in Figure 13: The relative differences in the fission rate follow the basic form of the relative differences in the neutron flux with some additional detail in the resolved resonance range due to widening of the resonance peaks in the fission cross section of ^{235}U.

The changes in the reaction rates and neutron flux are summarized in Table 2 for the thermal and fast energy regions. It is easy to see that the increasing fuel temperature leads to an increase in the fast capture rate and a decrease in the thermal capture rate as well as thermal and fast fission rates.

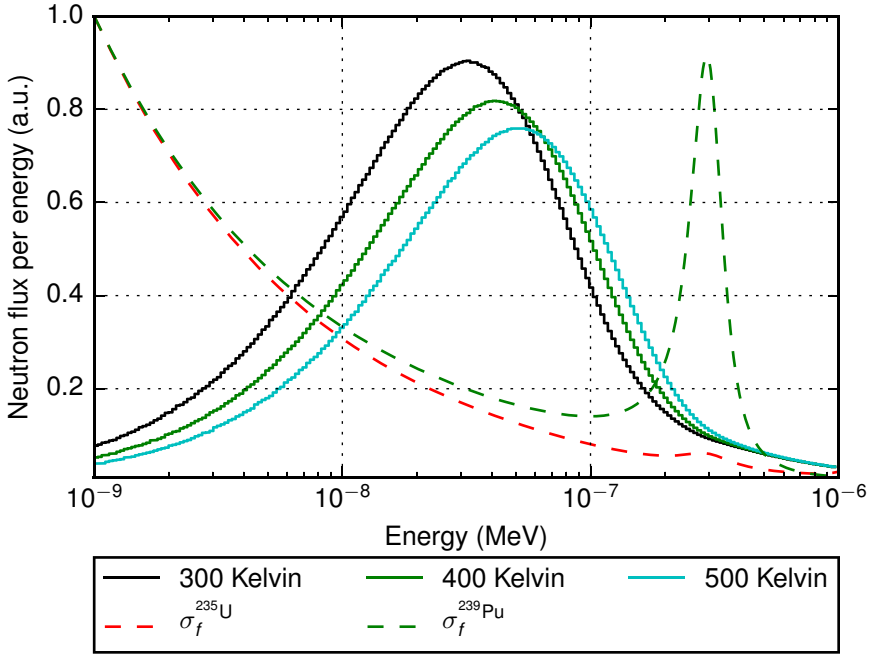

Figure 14. Shifting of the thermal peak with increasing moderator temperature. The shapes of ^{235}U and ^{239}Pu fission cross sections (scaled to 1.0 at 1×10^{-9} MeV) are plotted in the same figure with red and green dashed lines, respectively, using a linear scale for the y-axis.

4.3.2 Moderator temperature feedback

In light water reactors the water in the reactor core serves a dual purpose being both the coolant material and the moderator material. Since an increase in fission power will lead to an increase in the coolant material temperature, the moderating properties of the material will change at the same time as a result of the increased power.

The moderator temperature feedback effect in light water reactors means that an increase in the moderator temperature decreases the system reactivity. This purely temperature-related effect originates from the fact that as neutrons lose their energy in collisions with moderator atoms, they move towards a thermal equilibrium with the moderator material.

In an infinite moderator material without neutron loss or production, the neutron energy distribution would approach the Maxwell-Boltzmann distribution at the moderator material temperature. Although the reactor environment contains both neutron loss and production, which makes the situation more complex, the effect of this thermal equilibrium between low-energy neutrons and the moderator atoms can be seen in the fact that the energy-dependent neutron flux in a thermal reactor is at its highest at neutron energies close to the maximum of the Maxwell-Boltzmann distribution at the moderator temperature (see Fig. 4).

Fig. 14 shows the energy spectrum for the thermal energy range in the example geometry with different moderator temperatures. The movement of the thermal peak to higher energies with increasing moderator temperature can clearly be seen. Inspection of the fission cross section of ^{235}U, which is plotted in the same figure, shows that as the thermal peak moves to higher energies, the fission probability at the thermal peak also decreases leading to a decrease in system reactivity. It should be noted, however, that in the case of the fissile ^{239}Pu isotope, the displacement of the thermal peak to higher energies increases the overlap between the thermal peak and the 0.296 eV resonance peak in the ^{239}Pu fission cross section leading to an increase in the reactivity. For this reason, the moderator temperature feedback may be positive in systems in which the importance of ^{239}Pu fission is significant compared to the importance of ^{235}U fission.

4.3.3 Moderator density feedback

The moderator density feedback is independent of the moderator temperature feedback, although changes in the moderator density may be due to heating up of the material, causing both feedback effects to occur at the same time. Other notable reasons for changes in the moderator density without an associated change in the moderator temperature include sudden changes in the system pressure or boiling of the coolant, which is important in boiling water reactors.

As the density of the moderator decreases, the macroscopic cross sections for the moderator nuclides decrease (see Eq. 8). This results in longer mean-free-paths for the neutrons traveling in the moderator (see Eq. 7), which increases the probability of the neutrons returning to the fuel before they have sufficiently thermalized, leading to a decrease in the system reactivity.

It should be noted that if the moderator material contains a large amount of neutron-capturing nuclides (such as soluble boric acid), a decrease in the moderator

material density will also lead to a decrease in the neutron capture rate and may lead to a net positive moderator density feedback effect. This is mainly a possibility in storage and cold-zero-power conditions, in which a large amount of soluble neutron absorber is added to keep the system significantly subcritical.

4.3.4 Thermal mechanical feedbacks

The heating of the different parts of the nuclear reactor such as the fuel pellets, fuel rod cladding and assembly grid spacers brings about geometry changes resulting from thermal expansion. The uneven heating and different thermal expansion coefficients of the materials present in the reactor core results in uneven thermal expansion, which can have major effects on, for example the heat transfer in the fuel rods: During full power operation, the temperature of the nuclear fuel is hundreds of Kelvin higher than the temperature of the rod cladding. This results in the thermal expansion of the fuel pellet being significantly larger than that of the cladding, which leads to a decrease in the width of the gas gap in the fuel rod and an increase in the heat transfer between the fuel pellet and cladding.

The thermal expansion of the cladding can lead to a decrease in the flow area of the coolant (shown in blue in Figure 8) if the thermal expansion of the assembly spacing grids that control the pin pitch cannot counteract the expansion of the cladding. The decrease in the coolant flow area leads to a reduction in the neutron moderation in the fuel lattice, which will lead to a decrease in the reactivity.

4.4 Summary: Multi-physics coupling in thermal reactors

Figure 15 shows a schematic representation of the coupling between different physical fields in a thermal reactor core: The neutron flux distribution determines the power distribution in the reactor core, which acts as a source term for the thermal–hydraulic and thermal–mechanical phenomena in the core producing the temperature and density fields that in part affect the neutron flux distribution.

The cumulative effect of the feedback effects introduced in the previous sections means that the total power feedback effect is negative in all currently operating LWRs in their operating conditions. The implications of this are the following: If a critical reactor operating at the nominal power level is slightly perturbed by the addition of a small amount of positive reactivity, e.g. through a small retraction of the reactor control elements, the power level will initially start to increase slowly. However, as the power increases and the temperatures of the fuel and the coolant materials increase, the feedback effects will decrease the reactivity of the core and, eventually, fully counteract the added reactivity. At this point, the reactor will have reached a new stable power level slightly higher than the initial one.

Conversely, the addition of a small amount of negative reactivity will eventually lead to the stabilization of the system to a new power level slightly lower than the initial one.

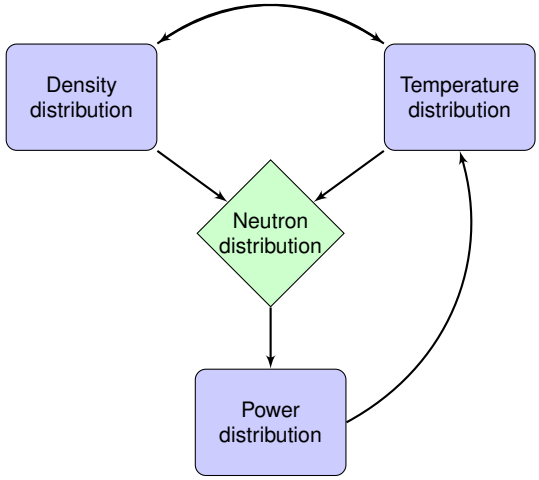

Figure 15. Schematic representation of the multi-physics coupling in a thermal reactor core.

5. Computational methods for multi-physics calculations

The feedback effects presented in the previous section indicate that there is a two-way coupling between the neutron flux and material temperature and density distributions. The result is that if an accurate realistic solution is required for one of the fields it has to be obtained to all of them. For example, one might want to obtain an accurate estimate of the maximum fuel temperature in the geometry presented in Fig. 8 at a specific linear power level and bulk coolant temperature. In order to calculate the temperature distribution inside the fuel rod, an accurate estimate for the fission power distribution inside the fuel rod is required, but as the fuel temperature affects the interaction probabilities in the fuel material, an accurate estimate of the fuel temperature distribution is required in order to calculate the fission power distribution.

This section presents the mathematical formalism of the multi-physics problem and the most common solution techniques used with deterministic solvers. The argumentation borrows heavily from the description of the multi-physics problem in the theory manual of LIME [18], the Lightweight Integrating Multi-physics Environment developed at Sandia National Laboratories.

5.1 Mathematical description of the multi-physics problem

In deterministic applications, a single physics can be described using a system of equations

$$\begin{aligned} f_1(\dot{u}_1, \dot{u}_2, \ldots, \dot{u}_{nu}, u_1, u_2, \ldots, u_{nu}, p_1, p_2, \ldots, p_{np}, t) &= 0 \\ f_2(\dot{u}_1, \dot{u}_2, \ldots, \dot{u}_{nu}, u_1, u_2, \ldots, u_{nu}, p_1, p_2, \ldots, p_{np}, t) &= 0 \\ &\vdots \\ f_{nu}(\dot{u}_1, \dot{u}_2, \ldots, \dot{u}_{nu}, u_1, u_2, \ldots, u_{nu}, p_1, p_2, \ldots, p_{np}, t) &= 0, \end{aligned} \tag{31}$$

where u are the state variables to be solved, $\dot{u}$ are their time derivatives, p are fixed parameters coming from other sources and t is the time coordinate. For example, u could be material temperatures at different locations, p could be heat production as well as material properties at different locations and f would be a set of energy conservation equations used to solve for the unknown variables. We shall denote an array of equations of the previous form with

$$\boldsymbol{f}(\dot{\boldsymbol{u}}, \boldsymbol{u}, \boldsymbol{p}, t) = 0, \tag{32}$$

where each of the bold symbols indicates an array (or a vector) of elements. For steady state applications, the previous equation becomes simpler:

$$\boldsymbol{f}(\boldsymbol{u}, \boldsymbol{p}) = 0. \tag{33}$$

We can now define the multi-physics problem. Let us say that

$$\boldsymbol{f}_1(\dot{\boldsymbol{T}}, \boldsymbol{T}, \boldsymbol{p}_1, t) = 0, \tag{34}$$

does indeed represent a system of energy conservation equations in some spatial domain, written for the material temperature distribution $\boldsymbol{T}$ and its time derivative. The parameters $\boldsymbol{p}_1$ are the heat conductivity distribution λ, the specific heat capacity distribution $\boldsymbol{c_v}$, the power density distribution $\boldsymbol{q}$ and possibly some additional parameters $\mathcal{P}_1$:

$$\boldsymbol{p}_1 = \{\lambda, \boldsymbol{c_v}, \boldsymbol{q}, \mathcal{P}_1\}.$$

If we assume that the parameters are independent of the $\boldsymbol{T}$ we can solve Eq. 34 as a single physics problem. However, as material thermal properties can be significantly dependent on temperature, we can write separate single physics equations for them:

$$\begin{aligned} \boldsymbol{f}_2(\lambda, \boldsymbol{p}_2) &= 0 \\ \boldsymbol{f}_3(\boldsymbol{c_v}, \boldsymbol{p}_3) &= 0 \end{aligned}$$

For this example, we can reasonably assume that the material properties are mostly dependent on the instantaneous temperature distribution and some additional model parameters:

$$\begin{aligned} \boldsymbol{p}_2 &= \{\boldsymbol{T}, \mathcal{P}_2\} \\ \boldsymbol{p}_3 &= \{\boldsymbol{T}, \mathcal{P}_3\}. \end{aligned}$$

The multi-physics problem then is to acknowledge the interdependence of these parameters by dividing the parameters $\boldsymbol{p}_i$ into the coupled parameters $\boldsymbol{z}_i$, that depend on the solution of the other physics problems, and the independent parameters $\boldsymbol{p}_i$, that are truly independent from the set of different physics problems that is being solved. Each single physics equation system (Eq. 32) is then transformed to the multi-physics form:

$$\boldsymbol{f}(\dot{\boldsymbol{u}}, \boldsymbol{u}, \boldsymbol{z}, \boldsymbol{p}, t) = 0. \tag{35}$$

Keeping to the multi-physics notation, our multi-physics problem for the heat conduction can be now expressed as

$$\begin{aligned} \boldsymbol{f}_1(\dot{\boldsymbol{T}}, \boldsymbol{T}, \{\lambda, \boldsymbol{c_v}\}, \{\boldsymbol{q}, \boldsymbol{p}_1\}, t) &= 0 \\ \boldsymbol{f}_2(\lambda, \boldsymbol{T}, \boldsymbol{p}_2) &= 0 \\ \boldsymbol{f}_3(\boldsymbol{c_v}, \boldsymbol{T}, \boldsymbol{p}_3) &= 0 \end{aligned} \tag{36}$$

In general then, a multi-physics problem can be expressed (as in Eq. 36) using a set of N physics equation systems

$$\begin{aligned} \boldsymbol{f}_1(\dot{\boldsymbol{u}}_1, \boldsymbol{u}_1, \boldsymbol{z}_1, \boldsymbol{p}_1, t) &= 0 \\ \boldsymbol{f}_2(\dot{\boldsymbol{u}}_2, \boldsymbol{u}_2, \boldsymbol{z}_2, \boldsymbol{p}_2, t) &= 0 \\ &\vdots \\ \boldsymbol{f}_N(\dot{\boldsymbol{u}}_N, \boldsymbol{u}_N, \boldsymbol{z}_N, \boldsymbol{p}_N, t) &= 0 \end{aligned} \tag{37}$$

to be solved in a self-consistent manner. We shall denote the group of all $\boldsymbol{u}_i$ with $\boldsymbol{U}$, and the group of all $\boldsymbol{p}_i$ with $\boldsymbol{P}$. As the $\boldsymbol{z}_i$ are functions of some $\boldsymbol{u}_k$ and some $\boldsymbol{p}_k$ we

can denote the previous set of equation systems in a slightly simpler form

$$\begin{aligned} \boldsymbol{g}_1(\dot{\boldsymbol{U}}, \boldsymbol{U}, \boldsymbol{P}, t) &= 0 \\ \boldsymbol{g}_2(\dot{\boldsymbol{U}}, \boldsymbol{U}, \boldsymbol{P}, t) &= 0 \\ &\vdots \\ \boldsymbol{g}_N(\dot{\boldsymbol{U}}, \boldsymbol{U}, \boldsymbol{P}, t) &= 0 \end{aligned} \tag{38}$$

which is then written simply as

$$\boldsymbol{F}(\dot{\boldsymbol{U}}, \boldsymbol{U}, \boldsymbol{P}, t) = 0, \tag{39}$$

where $\boldsymbol{F}$ represents the set of physics equations $\{\boldsymbol{g}_i\}$. In real applications, time discretization is applied to Eq. 39 and the system of equations to solve for a specific time step is

$$\boldsymbol{F}(\boldsymbol{U}, \boldsymbol{P}) = 0. \tag{40}$$

In the next sections we shall not write the constant parameter vector $\boldsymbol{P}$ as a part of the previous expression in order to simplify the upcoming equations, but the constant parameter vector will still be included in the equation system.

5.2 Fixed point iteration

One of the simplest approaches to multi-physics coupling is a fixed-point iteration, where the different solvers are executed consecutively keeping the coupled physics constant. This solution method uses a zeroth order approximation for the coupled physics in each of the solvers, but the consecutive execution of the solvers results in the convergence of the coupled solution.

Algorithm 2. Fixed point iteration in a single-physics application.

	Start with initial guesses $\boldsymbol{u}^{(0)}$.
	$k = 0$
1:	**while** not converged:
2:	$\quad \boldsymbol{u}^{(k+1)} = G(\boldsymbol{u}^{(k)})$
3:	$\quad k = k + 1$
4:	**end while**

The solution of a single-physics problem using fixed-point iteration is described in Algorithm 2: The solution scheme simply relies on obtaining a new iterate $\boldsymbol{u}^{(k+1)}$ from the previous iterate $\boldsymbol{u}^{(k)}$ using an operator G. The operator G is application specific, but can be as simple as evaluating the set of physical constraint equations $\boldsymbol{f}$. The fixed point iteration can be applied to multi-physics problems in various specific ways, but one of the simplest possibilities is detailed in Algorithm 3: In this variant, the individual operators G_i are often separate solvers for the separate physical

equation systems $\boldsymbol{f}_i$. The iteration itself then only consists of executing the different solvers in a consecutive manner and updating each of the solution fields $\boldsymbol{u}_i$ based on G_i.

Algorithm 3. One approach to the use of fixed point iteration in multi-physics.

Start with initial guesses $\boldsymbol{u}_1^{(0)}, \boldsymbol{u}_2^{(0)}, \ldots \boldsymbol{u}_N^{(0)}$.
$k = 0$
1: **while** not converged:
2: $\quad \boldsymbol{u}_1^{(k+1)} = G_1(\boldsymbol{u}_1^{(k)}, \boldsymbol{u}_2^{(k)}, \ldots, \boldsymbol{u}_N^{(k)})$
3: $\quad \boldsymbol{u}_2^{(k+1)} = G_2(\boldsymbol{u}_1^{(k+1)}, \boldsymbol{u}_2^{(k)}, \ldots, \boldsymbol{u}_N^{(k)})$
$\quad \vdots$
4: $\quad \boldsymbol{u}_N^{(k+1)} = G_N(\boldsymbol{u}_1^{(k+1)}, \boldsymbol{u}_2^{(k+1)}, \ldots, \boldsymbol{u}_N^{(k)})$
5: $\quad k = k + 1$
6: **end while**

The fixed point iteration is an easy way to couple pre-existing solvers, as the solvers G_i only need to provide the new solution for their individual physics $\boldsymbol{u}_i^{(k)}$ considering the other fields to be constant parameters. One of the main drawbacks of the fixed point iteration is the slow convergence rate of the algorithm [18].

5.3 Newton's method

Algorithms based on Newton's method linearize the non-linear equation system (Eq. 32) using a first order multivariate Taylor's expansion around the current solution point $\boldsymbol{U}^{(k)}$:

$$\boldsymbol{F}(\boldsymbol{U}) \approx \boldsymbol{F}(\boldsymbol{U}^{(k)}) + \boldsymbol{F}'(\boldsymbol{U}^{(\boldsymbol{k})})(\boldsymbol{U} - \boldsymbol{U}^{(k)}), \tag{41}$$

where the derivative of $\boldsymbol{F}$ is simply its Jacobian at the point

$$\boldsymbol{F}'(\boldsymbol{U}^{(k)}) = \boldsymbol{J}(\boldsymbol{U}^{(k)}) = \begin{bmatrix} J_{1,1} & \cdots & J_{1,N} \\ \vdots & \ddots & \vdots \\ J_{N,1} & \cdots & J_{N,N} \end{bmatrix}_{\boldsymbol{U}=\boldsymbol{U}^{(k)}} \tag{42}$$

shown here in the block-matrix format, where the blocks $J_{i,j}$ represent the sensitivities of the constraint equations from physics i ($\boldsymbol{f}_i$) to the state variables from physics j ($\boldsymbol{u}_j$):

$$J_{i,j} = \begin{bmatrix} \frac{\partial f_{i,1}}{\partial u_{j,1}} & \cdots & \frac{\partial f_{i,1}}{\partial u_{j,N_{j,1}}} \\ \vdots & \ddots & \vdots \\ \frac{\partial f_{i,N_{i,1}}}{\partial u_1} & \cdots & \frac{\partial F_{N_{i,1}}}{\partial u_{j,N_{j,1}}} \end{bmatrix}_{\boldsymbol{u}_j=\boldsymbol{u}_j^{(k)}}. \tag{43}$$

The next estimate for the solution of Eq. 40 can be obtained by solving for the next iterate from the linear model:

$$\boldsymbol{F}(\boldsymbol{U}^{(k)}) + \boldsymbol{J}(\boldsymbol{U}^{(k)})(\boldsymbol{U}^{k+1} - \boldsymbol{U}^{(k)}) = 0 \tag{44}$$

$$\boldsymbol{J}(\boldsymbol{U}^{(k)})\boldsymbol{x} = -\boldsymbol{F}(\boldsymbol{u}^{(k)}), \tag{45}$$

from which the next step in the solution space $\boldsymbol{x} = \boldsymbol{U}^{k+1} - \boldsymbol{U}^{(k)}$ can be solved using suitable linear algebra tools.

Algorithm 4. Use of Newton's method in multi-physics.

Start with an initial guesses $\boldsymbol{U}^{(0)}$.
$k = 0$
1: **while** not converged:
2: $\quad \boldsymbol{x} \leftarrow \boldsymbol{J}(\boldsymbol{U}^{(k)})\boldsymbol{x} = -\boldsymbol{F}(\boldsymbol{U}^{(k)})$
3: $\quad \boldsymbol{U}^{(k+1)} = \boldsymbol{U}^{(k)} + \boldsymbol{x}$
4: $\quad k = k + 1$
5: **end while**

The application of Newton's method for multi-physics problems is outlined in Algorithm 4. The derivative terms of the Jacobian can be calculated analytically or by finite difference approximation, e.g. by using forward difference:

$$\frac{\partial f_i(\boldsymbol{U}^{(k)})}{\partial u_j} = \frac{f_i(\boldsymbol{U}^{(k)} + \delta\hat{\boldsymbol{e}}_j) - f_i(\boldsymbol{U}^{(k)})}{\delta}, \tag{46}$$

where $\hat{e}_j$ is the unit vector in the direction of u_j.

One downside of the standard Newton's method is the need to construct the full Jacobian matrix. If the dimension of the original problem is large, calculating and storing the matrix can be expensive and prone to error. However, as the next section shows, solution schemes exist that apply Newton's method without the need to construct and store the full Jacobian.

5.4 Jacobian-free Newton–Krylov

Knoll and Keyes [19] provided a thorough overview of the Jacobian-free Newton–Krylov (JFNK) methods, but a short overview is given here as JFNK is a popular approach to multi-physics problems in the case of deterministic solvers. The idea behind JFNK is to solve step 2 of Newton's method (Algorithm 4) using a Krylov-subspace method, in which the Krylov-subspace is spanned by

$$\boldsymbol{K}_j = \text{span}\left(\boldsymbol{r}_0, \boldsymbol{J}\boldsymbol{r}_0, \boldsymbol{J}^2\boldsymbol{r}_0, \ldots, \boldsymbol{J}^{j-1}\boldsymbol{r}_0\right), \tag{47}$$

where

$$\boldsymbol{r}_0 = -\boldsymbol{F}(\boldsymbol{U}^{(k)}) - \boldsymbol{J}\boldsymbol{x}_\mathbf{0} \tag{48}$$

is the residual of Eq. 45 with an initial guess $\boldsymbol{x}_0$. The main attraction of the Krylov-methods in the context of the multivariate Newton's method is the fact that they can be used to solve linear equations of the form

$$\boldsymbol{A}\boldsymbol{x} = \boldsymbol{b} \tag{49}$$

without the need to explicitly form the matrix $\boldsymbol{A}$. Only a number of matrix-vector products need to be formed for $\boldsymbol{A}$. In the case of Newton's method, the matrix $\boldsymbol{A}$ is the Jacobian in Eq. 45, which means that only a number of vector products of the form $\boldsymbol{J}\boldsymbol{v}_k$ have to be calculated for the Jacobian. These are essentially directional derivatives of the initial equation system, and can be either evaluated analytically or approximated with finite differences:

$$\boldsymbol{J}\boldsymbol{v}_k = \frac{\boldsymbol{F}(\boldsymbol{U} + \delta\boldsymbol{v}_k) - \boldsymbol{F}(\boldsymbol{U})}{\delta}. \tag{50}$$

In this way, the JFNK methods can utilize Newton's method for solving complex multi-physics problems without the need to calculate and store the full Jacobian.

6. Multi-physics with Monte Carlo particle tracking

Coupling the Monte Carlo neutron tracking to other solvers in a multi-physics framework is challenging, since much of the formalism presented in Section 5 does not directly apply to Monte Carlo neutronics; the Monte Carlo neutron tracking does not solve any equation system written for the neutron flux distribution to obtain the solution. Instead the Monte Carlo neutron transport solution can be seen as a general operator $\mathbb{M}$, which takes in the dependent parameters $\boldsymbol{z}_M$, for example material temperature and density distributions, as well as a group of independent parameters $\boldsymbol{p}_M$ and provides a vector of results:

$$\hat{\boldsymbol{u}}_M = \mathbb{M}(\boldsymbol{z}_M, \boldsymbol{p}_M) \tag{51}$$

Here the operation $\mathbb{M}(\boldsymbol{z}_M, \boldsymbol{p}_M)$ refers to executing the Monte Carlo simulation (in k-eigenvalue or fixed source mode) and the result vector $\hat{\boldsymbol{u}}_M$ could generally contain statistical estimates for various result variables such as power distribution or neutron flux distribution tallied in a variety of spatial cells, multiplication factor of the system etc. In the following discussion, however, we shall only include the power distribution in $\hat{\boldsymbol{u}}_M$.

Applying Newton's method to a problem requires evaluating the residual of the multi-physics equation system (right hand side of Eq. 45), which requires evaluating the residuals for the partial single-physics problems. Although there has been success in the development of residual Monte Carlo methods for specific applications (see e.g. [20], [21] and[22]), these methods have yet to be applied to the continuous energy Monte Carlo neutron transport methods used in this work.

A second challenge for Monte Carlo multi-physics is the fact that the power distribution $\hat{\boldsymbol{u}}_M$ obtained from the Monte Carlo simulation is only a statistical estimate for the actual result $\boldsymbol{u}_M$ and contains an additional stochastic error term ε

$$\hat{\boldsymbol{u}}_M = \boldsymbol{u}_M + \varepsilon. \tag{52}$$

As there is no functional dependence between the coupled fields and the result distribution, there is no possibility to evaluate the derivatives required for the Jacobian in the Newton's method analytically and due to the stochastic error term present in the Monte Carlo solution, the evaluation of finite differences requires a large number of neutron histories in order to obtain reliable estimates for the sensitivities. Due to the computational cost of the Monte Carlo transport solution, evaluating thousands or millions of sensitivities for a single coupled-calculation iteration is not a realistic possibility if each sensitivity has to be evaluated with a separate simulation. The use of Newton's method with continuous energy Monte Carlo neutron transport can be challenging[8].

Monte Carlo neutronics can be used as a part of a fixed point iteration scheme (Algorithm 3). The Monte Carlo operator $\mathbb{M}$ will then approximate one of the G_i operators for the fixed point iteration with a stochastic operator $\hat{G}_M(\boldsymbol{U}) = G_M(\boldsymbol{U}) + \varepsilon(\boldsymbol{U})$. The application of this operator on the current solution vector $\boldsymbol{U}$ (containing, e.g. the material temperatures and densities calculated based on the previous power

[8] Newton's method or JFNK can, however, be used for the other fields of coupled physics even when the power distribution is supplied by Monte Carlo neutronics.

distribution) requires executing the Monte Carlo simulation and will yield the next stochastic estimate for the power distribution $\hat{\boldsymbol{u}}_M$:

$$\hat{\boldsymbol{u}}_M^{(k+1)} = \hat{G}_M(\boldsymbol{U}^{(k)}), \tag{53}$$

where the right hand size is evaluated by running the Monte Carlo simulation.

In fixed point iteration the conventional practice is to estimate the convergence of the coupled problem by monitoring the differences in fields between two subsequent iterations[9]

$$\left\| \boldsymbol{u}_i^{(k+1)} - \boldsymbol{u}_i^{(k)} \right\| = \left\| G_i(\boldsymbol{u}_i^{(k)}) - \boldsymbol{u}_i^{(k)} \right\|, \tag{54}$$

which should tend towards zero as the iteration tends towards the correct solution. For the Monte Carlo neutron transport solution, the difference will be limited by the stochastic error terms

$$\left\| \hat{\boldsymbol{u}}_M^{(k+1)} - \hat{\boldsymbol{u}}_M^{(k)} \right\| = \left\| \hat{G}_M(\hat{\boldsymbol{u}}_M^{(k)}) - \hat{\boldsymbol{u}}_M^{(k)} \right\| = \left\| G_M(\boldsymbol{u}_M^{(k)} + \boldsymbol{\epsilon}^{(k)}) + \boldsymbol{\epsilon}^{(k+1)} - (\boldsymbol{u}_M^{(k)} + \boldsymbol{\epsilon}^{(k)}) \right\|, \tag{55}$$

which can be decreased by using a large number of source particles in the simulation but cannot be completely eliminated. The stochastic approximation-based solution techniques presented in the next section attempt to find a way around these difficulties.

6.1 Stochastic approximation-based solution techniques

In the stochastic approximation approach, the coupled problem can be reformulated around the Monte Carlo transport operator described in Eq. 53.

The problem is to find the converged solution for the power distribution ($\boldsymbol{u}_M$) so that

$$G_M(\boldsymbol{u}_1^{(k+1)}, \boldsymbol{u}_2^{(k+1)}, \dots, \boldsymbol{u}_M^{(k)}, \dots, \boldsymbol{u}_N^{(k)}) = \boldsymbol{u}_M^{(k+1)} = \boldsymbol{u}_M^{(k)}, \tag{56}$$

i.e. the calculation (G_M) of the new power distribution using the coupled fields ($\boldsymbol{u}_i$, where $i \neq M$) calculated using the previous power distribution $\boldsymbol{u}_M^{(k)}$ yields a power distribution equal to the one obtained on the previous step.

The power distribution $\boldsymbol{u}_M^{(k)}$ will also be the solution for the minimization problem

$$\min f(\boldsymbol{u}_M^{(k)}) = \min \left\| G_M(\boldsymbol{u}_1^{(k+1)}, \boldsymbol{u}_2^{(k+1)}, \dots, \boldsymbol{u}_M^{(k)}, \dots, \boldsymbol{u}_N^{(k)}) - \boldsymbol{u}_M^{(k)} \right\|_2, \tag{57}$$

which minimizes the ℓ^2 norm of the residual field of Eq. 56. The problem is that the operator G_M can be accessed only through the stochastic estimate $\hat{G}_M$. Luckily, the Robbins–Monro algorithm [23] for stochastic approximation was developed for exactly such problems.

Dufek and Gudowski [24] showed that the stochastic approximation can be applied to the calculation of the multi-physics problem with Monte Carlo neutronics in steady state. They showed that with slight approximations based on the localized and negative feedback effects between the neutron flux and the coupled fields, the Robbins-Monro algorithm for the Monte Carlo multi-physics can be worked to

$$\boldsymbol{u}_M^{(k+1)} = \boldsymbol{u}_M^{(k)} - a_k d \left(\boldsymbol{u}_M^{(k)} - \hat{G}_M(\boldsymbol{u}_1^{(k+1)}, \boldsymbol{u}_2^{(k+1)}, \dots, \boldsymbol{u}_M^{(k)}, \dots, \boldsymbol{u}_N^{(k)}) \right), \tag{58}$$

[9] It should be noted that this conventional approach has a risk of providing a false prediction of convergence.

where a_k is the step size at step k and d is an under-relaxation factor. There are several ways to choose the step size a_k: Robbins and Monro used

$$a_k = \frac{C}{k}, \tag{59}$$

where C is a constant. Dufek and Gudowski suggested that in the Monte Carlo context, a good choice for the step size would be

$$a_k = \frac{s_k}{\sum_i^k s_i}, \tag{60}$$

where s_i is the simulated active neutron population at step i. The step size for step k would then be the number of active histories simulated on step k divided by the sum of active histories simulated on previous steps up to and including k. The operation of stochastic approximation methods in this context can then be summarized in Algorithm 5.

Algorithm 5. Use of stochastic approximation in multi-physics as a part of a fixed point iteration scheme. $\boldsymbol{u}_M$ is the solution of the Monte Carlo neutron transport simulation. The execution of the MC simulation is denoted by the stochastic operator $\hat{G}_M$.

Start with initial guesses $\boldsymbol{u}_1^{(0)}, \boldsymbol{u}_2^{(0)}, \ldots, \boldsymbol{u}_M^{(0)}, \ldots, \boldsymbol{u}_N^{(0)}$.
$k = 0$

while not converged:
  $\boldsymbol{u}_1^{(k+1)} = G_1(\boldsymbol{u}_1^{(k)}, \boldsymbol{u}_2^{(k)}, \boldsymbol{u}_M^{(k)}, \ldots, \boldsymbol{u}_N^{(k)})$
  $\boldsymbol{u}_2^{(k+1)} = G_2(\boldsymbol{u}_1^{(k+1)}, \boldsymbol{u}_2^{(k)}, \boldsymbol{u}_M^{(k)}, \ldots, \boldsymbol{u}_N^{(k)})$
  ⋮
  $\boldsymbol{x}^{(k+1)} = \hat{G}_M(\boldsymbol{u}_1^{(k+1)}, \boldsymbol{u}_2^{(k+1)}, \ldots, \boldsymbol{u}_M^{(k)}, \ldots, \boldsymbol{u}_N^{(k)})$
  $\boldsymbol{u}_M^{(k+1)} = \boldsymbol{u}_M^{(k)} - a_k d(\boldsymbol{u}_m^{(k)} - \boldsymbol{x}^{(k)})$
  ⋮
  $\boldsymbol{u}_N^{(k+1)} = G_N(\boldsymbol{u}_1^{(k)}, \boldsymbol{u}_2^{(k)}, \ldots, \boldsymbol{u}_M^{(k+1)}, \boldsymbol{u}_N^{(k)})$
  $k = k + 1$
end while

6.2 Changes required to MC algorithms

Hitherto, we have assumed the existence of a Monte Carlo neutron transport operator $\mathbb{M}$ that is capable of providing a high-fidelity neutron transport solution $\boldsymbol{u}_M$ based on the coupled fields provided by the other solvers $\boldsymbol{U}$. Monte Carlo neutron transport relies on basing the random sampling in the simulation on the neutron cross sections $\sigma(E)$ and $\Sigma(E)$ that were largely considered to be constant for each material

region when discussing the Monte Carlo neutron transport in Section 3. However, Section 4.3 established that the interaction probabilities (the cross sections) are strongly dependent on material temperature and density:

$$\sigma = \sigma(E, T)$$
$$\Sigma = \Sigma(E, T, \rho) = \sigma(E, T)N(\rho)$$

In multi-physics applications the temperature and density fields may be supplied to the Monte Carlo code by other solvers as a high-fidelity distribution. The Monte Carlo code should then be able to simulate the random walk of neutrons efficiently even if the distributions are rather complex. There are several parts of the Monte Carlo neutron transport process that must be adapted for multi-physics applications as described in the following sections.

6.2.1 Thermal effects on cross sections

Due to the temperature effects on the microscopic cross sections, the Monte Carlo code needs a way to evaluate the microscopic cross sections at the temperatures that the neutrons may encounter in the calculation model. The cross section temperature treatment approaches can be divided into pre-processing and on-the-fly methods: Pre-processing methods, as their name suggest, generate the cross section data for each required temperature before the start of the calculation using, for example, the NJOY code [25]. All of the cross section data is then loaded into the program memory for rapid access during the simulation. On-the-fly methods, on the other hand, operate with a reduced number of *base* cross section libraries at specified *base* temperatures and account for the temperature effect between the simulation temperature and the base temperature at runtime (on-the-fly).

Pre-processing the cross sections is only feasible in systems with a limited number of temperatures as each new temperature requires pre-processing and storing an additional set of cross sections. As the number of temperatures increases, so does the memory consumption. Another drawback for the pre-processing approach is the fact that, when the temperatures in the simulation change during the multi-physics solution process, the cross section data has to be pre-processed again, thus increasing the computational effort.

Multi-physics simulations using high-fidelity (or continuous) temperature fields are only feasible with the use of on-the-fly temperature treatment methods. The first on-the-fly approaches did not even try to evaluate the cross sections at the correct temperature. Instead they relied on generating temperature-dependent cross sections for a set of temperatures and then either

- simply using the closest temperature, **or**,
- interpolating between the bracketing temperatures, **or**,
- using *stochastic mixing* to ”interpolate” between the bracketed temperatures.

The first possibility is not generally applicable to multi-physics problems, in which accurate results are needed over wide temperature ranges but it was applied as an approximation in [4] and [5]. The accuracy of the second approach was studied by Trumbull in [26] and found to be rather poor. The stochastic mixing is possibly the first widely used and feasible approach to reconciling the temperature effects with a

reasonable number of pre-generated cross section libraries. In the stochastic mixing approach, materials between the base temperatures are modeled as mixtures of materials at the base temperatures. For example, water at 506 K might be approximated with a mixture of water at 500 K and water at 510 K. Although the approach is non-physical, it has produced reasonable results in a number of test cases and many researchers applied it as an approximation due to its simplicity (for example in [3, 5, 6, 27]) before the arrival of the more advanced on-the-fly techniques.

The second group of on-the-fly temperature treatment techniques endeavors to solve the temperature-dependent cross section at the target temperature using techniques similar to those used in NJOY, but during the neutron transport simulation. Two such methods are the approach proposed by Li [28] and the method implemented to the BINGO collision processor in the Monte Carlo code MONK [29]. For a discussion of the differences in the performance of these methods the reader is directed to a recent article by Romano and Trumbull [30].

In recent years several advanced approaches to the problem have been developed, including the following three:

- Use a single set of base cross sections and generate a series expansion for the temperature dependence and quickly calculate the temperature-dependent cross sections on-the-fly [31]. The method is used in MCNP6.
- Store a single set of base cross sections in multipole representation rather than pointwise tabulated format and calculate the analytical Doppler broadening on-the-fly [32]. This approach has been implemented in the OpenMC Monte Carlo code.
- Use a single set of base cross sections and take the temperature effect into account on-the-fly using the physical Target Motion Sampling temperature treatment technique [33]. This approach is used in the Serpent 2 Monte Carlo code.

The calculations in this work used the Target Motion Sampling (TMS) temperature treatment technique previously implemented in Serpent.

6.2.2 Effects on track length sampling

As was described in Section 3.2: track-lengths for neutrons can be sampled using Eq. 19, and the equation only applies if the cross section in the denominator is constant over the sampled track-length. Material boundaries are handled either by stopping the track-lengths at material interfaces and sampling a new track-length in the upcoming material (surface tracking), or by using a common majorant cross section for the track-length sampling in all materials and using the concept of virtual collisions to conserve the physics of the sampling (delta-tracking).

As the material temperature affects the material cross sections it is evident that the cross section in the denominator of Eq. 19 will depend on the material temperature, and even the different temperature regions of one material should be treated as different materials in the track-length sampling. With high-fidelity temperature distributions (see Fig. 16), the efficiency of surface tracking may become very poor if no modifications are made. The same is true in the case of high fidelity density distributions.

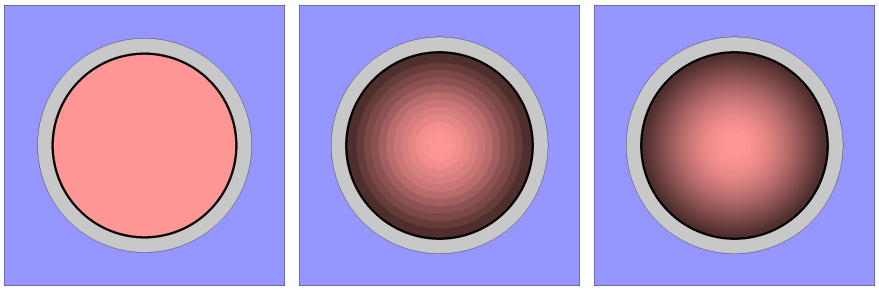

Figure 16. Pin-cell geometry with fuel temperature shown as shading. **Left**: Radially constant fuel temperature. **Center**: Radial temperature step profile. **Right**: Radially continuous temperature profile.

The simple solution for sampling track-lengths in materials with very refined or even continuous temperature and density distributions is to utilize rejection sampling in the track-length sampling [34, 35]. This approach uses a material-wise majorant cross section $\Sigma_{\text{maj.},*,t}(E)$ that covers the range of temperature and density variation for the material. These material-wise majorants are then used in track-length sampling inside the material region and the physics of the system are conserved by rejecting some of the sampled collision points. As this rejection sampling is used *inside* each material region, it can be used with both the surface tracking and Woodcock delta-tracking methods that handle the variation of the cross sections *between* the material regions.

6.2.3 Scoring tallies

There will be no changes required to the scoring of analog estimators. For collision estimators, the cross sections in the denominator of the tallied value (Eq. 28) will be temperature dependent and the nominator will be the multi-physics majorant for the local material (introduced in section 6.2.2) that is used for the track-length sampling inside the material:

$$\frac{\Sigma_t^{^1\text{H}}(E, T, \vec{r})}{\Sigma_{\text{maj.},*,t}(E)}. \tag{61}$$

The temperature-based cross section must be evaluated on-the-fly using the temperature at the interaction site. The tallied value for the track-length estimator is changed in the same way

$$\sum_i^{\text{materials}} \sum_j^{\text{temperatures}} \frac{\Sigma_{t,i,j}^{^1\text{H}}(E, T, \vec{r})}{\Sigma_{\text{maj.},*,i,t}(E)} s_i \tag{62}$$

and the previous track-length must be segmented not only based on the material region as in Eq. 30, but also based on the material temperature. The macroscopic cross sections of the material are constant over the track-length only if both the material and the material temperature are constant over the track-length. Track-length estimators can be used with arbitrarily refined, but not continuous, temperature and density distributions although their performance may be compromised if a

very large number of temperature/density region boundaries is crossed by the mean track-lengths of neutrons in the system.

6.2.4 Temperature and density distribution handling

The traditional approaches for defining the temperatures and densities in the Monte Carlo geometry have been to bind the temperature distribution to materials and the density distribution to either geometry cells or materials. This ensures that each geometry cell has a constant microscopic and macroscopic cross sections.

However, with the use of collision estimators the temperatures and densities are only required by the code at the interaction sites, which gives considerable freedom for the functional forms that can be used to represent the temperature and density distributions: Any function that translates coordinates into temperature and density information can be used. With track-length estimators the functions have the additional constraint of needing to yield step profiles, when evaluated over neutron tracks.

The traditional material and geometry cell-based temperature distributions can obviously be used in the multi-physics simulations, but the temperature and density information can also be separated from the underlying geometry. This means that, if the multi-physics interface of the Monte Carlo code is designed appropriately, changes in the temperature or density meshing do not necessitate changes in the Monte Carlo geometry model. The changes in the meshing might be simply changes in the mesh size (Fig. 17 left to center)) or even changes in the external solver from a structured mesh-based solver to a solver providing the fields using point fields instead of structured meshes (17 right). The possibility for the neutronics model to be agnostic of the coupled solver and to use the supplied distributions as-is, without cumbersome grid matching, is a major advantage of this kind of multi-physics approach.

It takes no additional effort to model temperature and density distributions that are continuous in space and time. The work in this thesis has utilized this fact via the use of radially continuous temperature distributions given either in functional form (Publication **I**) or using linear interpolation with respect to space (Publications **III**, **V** and **VI**) and time (Publication **III**). Continuous temperature representations have also been used with the OpenMC Monte Carlo code in combination with functional expansion tallies [36].

6.2.5 Providing external solvers with power distributions

As a part of multi-physics calculation sequence, the Monte Carlo code is required to provide a power distribution to the other codes in the calculation sequence. Providing an accurate heat deposition distribution for all of the associated materials is a complex task as heat is deposited, not only in fissions, but also in neutron and photon reactions with fuel, moderator, control rod and structural materials. The direct heating in moderator, control rod and structural materials is an important source term for thermal-hydraulic calculations. For accurate representation, the prompt energy deposition by neutrons and photons needs to be tallied, for example using the kinetic energy release per unit mass (KERMA) coefficients for each material of in-

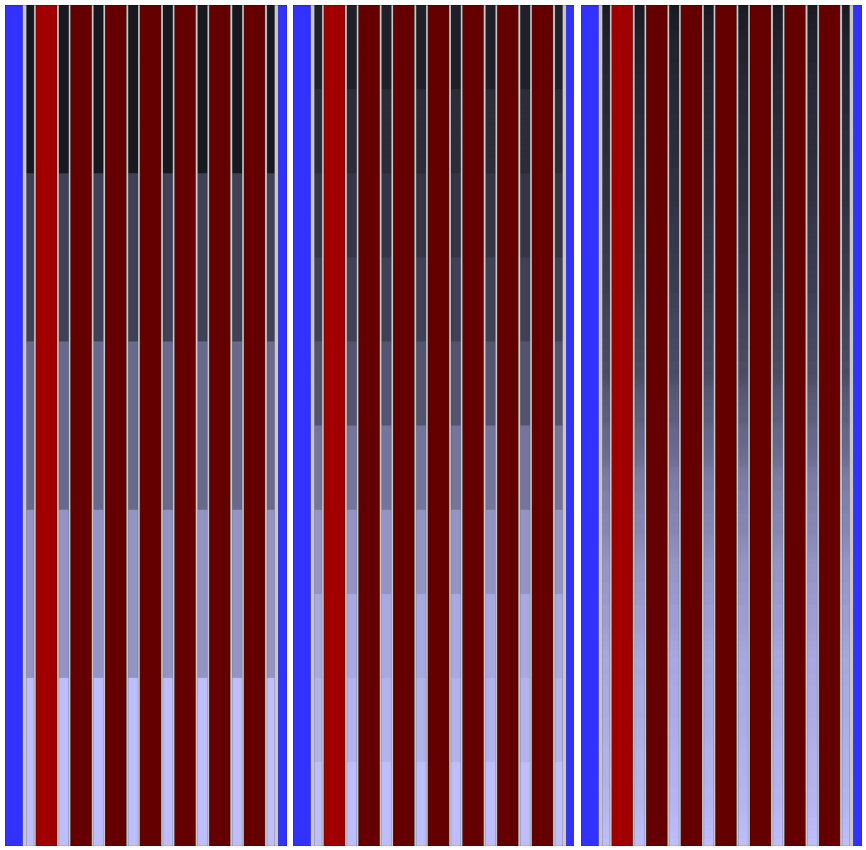

Figure 17. Serpent 2 YZ-geometry plots with different coolant density distributions provided by an external solver. Darker color indicates lower density. A well designed multi-physics approach means that no changes are required in the neutron transport geometry model if e.g. the meshing of the external solver changes (left to center) or if the external solver is swapped for one that provides the data as a point-field instead of on a structured mesh (right).

terest. This will require both a neutron and a photon transport calculation. The information on the prompt heating then needs to be combined with the calculation of the decay heat produced by decaying fission products.

The calculations conducted in this thesis were coupled calculations with fuel behavior solvers, for which only the heat generation in the fuel material was provided. The heat generation in the fuel was approximated by using a fixed value for local heat deposition due to one fission (κ), which for ^{235}U was 202.27 eV, the default value used by Serpent. For other fissionable nuclides the κ was scaled based on their fission Q-value

$$\kappa_n = \frac{Q_n}{Q_{\mathrm{U5}}} \kappa_{\mathrm{U5}}, \tag{63}$$

where the lower index U5 refers to ^{235}U. This approximation does not consider the accurate direct heat deposition of neutrons, photons or beta-particles, which is a potential topic for future improvement.

6.3 Application to time-dependent problems

An inherent advantage of the use of Monte Carlo codes in multi-physics simulations is the fact that Monte Carlo codes can easily be made to be inherently four dimensional. As the particle is moved in space between two interactions it can also be moved in time. By keeping track of the ”internal clock” of each neutron during the random walk, the time-dependent behavior of the particle population can be directly modeled without the need to solve the time-dependent behavior as a time-integral based on solutions at discrete time points.

As described by Bart Sjenitzer in his PhD thesis on the development of a dynamic Monte Carlo method [37], practical time-dependent multi-physics calculations with Monte Carlo neutronics typically require two additional implementations to the Monte Carlo code: First, a possibility should exist to divide the simulated time period into time intervals with a possibility for particle population control and data exchange with coupled codes at the time interval boundaries. Second, a model for tracking the delayed neutron precursors should be utilized instead of generating delayed neutrons directly from fissions.

A dynamic simulation mode based on the external source simulation mode with population control at time interval boundaries was implemented in Serpent in [38]. The mode was reworked to allow for time-dependent coupled calculations and demonstrated using the internally coupled fuel behavior module FINIX in a fast transient scenario without delayed neutron emission in Publication **III**. Delayed neutron precursor tracking and emission routines were later implemented and described in Publication **IV**. The implemented delayed neutron routines used an automatic group structure based on the cross section libraries chosen by user and the fissionable nuclides present in the problem.

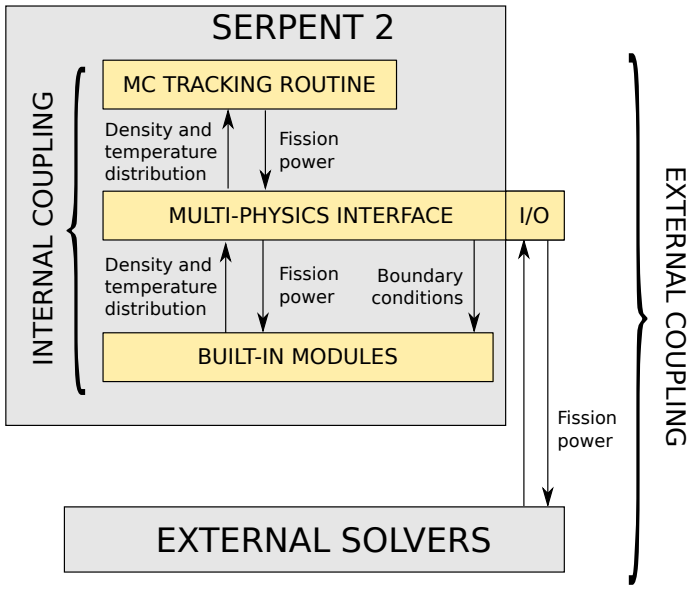

Figure 18. The two level coupling scheme in Serpent 2. Built-in solver modules can be used to obtain fast solutions for fuel and coolant behavior and high-fidelity solutions from state-of-the-art external solvers can be imported via the universal multi-physics interface.

7. Development of coupled calculation capabilities for Serpent 2

This section discusses the development and implementation of the coupled calculation capabilities of Serpent 2 in this thesis, whereas the next section (Section 8) will discuss the application of these capabilities to the problem of effective fuel temperatures. Although the development of the capabilities and their application did go hand-in-hand during the thesis work, a clearer picture of each topic can be given by focusing on one of the topics at a time.

7.1 Design choices

The goal of this thesis was to design the coupled calculation capabilities of Serpent 2 [8], a continuous energy Monte Carlo burnup code, in a sustainable manner. Sustainable, in the sense that the design choices and implementations would allow multi-physics simulations for a variety of simulation types in a code agnostic sense, while being easily extendable for future applications. The main simulation types that were included in the goals of the coupled calculation development were:

1. Steady state calculations using the criticality source simulation (k-eigenvalue) mode.

2. Burnup calculations.
3. Time-dependent simulations.

Relatively early in the development of Serpent 2, the design choice was made [39] to utilize a two-level coupling scheme (see Fig. 18), in which internal light-weight solvers could be used to obtain rapid solutions for fuel and coolant behavior and external state-of-the-art solvers could be coupled to Serpent via a universal code-agnostic multi-physics interface to provide truly high-fidelity solutions for the coupled fields. The approach taken in the implementation of the two-level coupling scheme in this work was to have the external and internal coupling to operate as similarly to each other as possible, i.e. to use the same sub-routines and data-structures whenever possible. Developing, implementing and maintaining a single set of sub-routines was the preferred approach from the point of view of code development.

The two level coupling scheme also eased the testing of the internal and external interface routines as they could be used for cross-verification as the two were applied to the same problem. The testing of the coupled calculation routines was mainly conducted via a set of test problems designed to test separate parts of the implementations (unit testing). These test problems were executed each time a version of Serpent was publicly distributed.

In 2012, when this thesis work began, Serpent had the physics models for handling the complex temperature and density distributions required in the multi-physics simulations, but the coupled calculation routines were still in their infancy. The first multi-physics interface types were included in Serpent 2.1.3, released in March 2012, for bringing in temperature and density data using point-fields or regular meshes, but no real coupled calculations were executed at the time. The first approach to an internally coupled calculation (Publication **I**) was developed in parallel with the first interface types.

7.2 First approach to internal coupling and steady state calculations

In Publication **I** the recently implemented TMS on-the-fly temperature treatment was applied to an actual coupled problem by implementing an internal analytic radial fuel temperature solver for UO_2 fuel rods and using the solver in a coupled calculation of a two-dimensional BWR assembly geometry at full power. Serpent tallied the radial fission power distribution in each fuel rod, whereas the implemented solver gave a solution for the time-independent radial heat equation in the cylindrical geometry of the fuel rod. The solver considered the temperature dependence of the heat conductivity of each material as well as the radial changes in the fuel rod geometry due to thermal expansion and pellet relocation. The possibility to apply the changes in the radial geometry of the fuel rod to the Monte Carlo geometry model was a notably novel approach, which makes it possible to estimate the effects that these changes have on the coupled solution.

This first coupled calculation implementation used a simple fixed point iteration (Algorithm 3 on page 50) until a convergence was reached between neutronics and fuel behavior. The coupled calculation iteration was executed after the simulation of each neutron batch. The fuel behavior was solved as a separate fixed point iteration between the temperature solution, the temperature-dependent material properties and the temperature-dependent radial changes in fuel rod geometry.

The internal fuel temperature solver proved to be successful in solving the coupled problem between fuel temperature and neutronics, although it was later replaced with the newly developed FINIX fuel behavior module for multi-physics applications [40, 41].

7.3 First approach to external coupling and burnup calculations

The calculation routines for external coupling were developed next in the context of externally coupled burnup calculations with the ENIGMA [42] fuel performance code in Publication **II**. For this purpose, several new capabilities were developed and implemented into Serpent, including

- The universal fuel performance code interface, also known as the fuel behavior interface and used in Publications **II**, **V** and **VI**. Many of the fuel performance code interface routines were also used by the internal FINIX fuel behavior module in Publication **III**.
- Radial coordinate transformations inside fuel rods to simulate modifications to the radial geometry in the fuel rods in the neutron tracking.
- POSIX-signalling capabilities and the ability to function as a part of an iterative coupled calculation scheme, without the need to restart Serpent for each iteration.

The fuel behavior interface allowed Serpent to read in the radial temperature and strain distributions for fuel rods at different axial elevations and overlay the distributions on the geometry model. On the other hand, the fuel behavior interface would automatically tally the radial fission power distribution at different axial elevations and write the power distribution to a file to be read by the external code. Two options were implemented for the functional form of the radial temperature profile: a step profile and linear interpolation between point-wise values.

The pre-processing of the problem geometry, material compositions and cross sections required for the neutron transport simulation takes a considerable time, especially in burnup calculations with a large number of transport nuclides. In order to increase the computational efficiency, several routines were implemented which made it possible to wait for the solution for coupled fields and read in updated distributions without the need to terminate and restart Serpent in between. In publication **II**, these newly developed capabilities were demonstrated in a coupled burnup calculation of a short VVER-440 type fuel assembly with burnable absorber rods. The coupling was extremely simple, as was also denoted in the publication, consisting simply of a single fixed-point iteration between the two solvers for each burnup step. As the two solutions were not iterated to convergence, the time-coupling can be described as a loose coupling.

7.4 Capabilities for time-dependent simulations

After the initial implementations of coupled calculation routines for steady state and burnup calculations, Publication **III** tackled the coupled time-dependent problem using the internally coupled FINIX fuel behavior module. A time-dependent simulation

mode had previously been implemented in Serpent [38], but in Publication **III** it was reworked to support coupled calculations. The new transient simulation mode was applied to a coupled simulation of a super-prompt critical transient in a 2D PWR pin-cell geometry. The coupled solution scheme was slightly more advanced than in the earlier publications: A fixed point iteration was used between the two solvers, with stochastic approximation-based solution relaxation applied to the power distribution solved by Serpent. Each time interval was iterated until the maximum difference in the end-of-interval fuel temperature distribution between two subsequent iterations was below 3 K. Due to this iteration, the time-coupling can be described as a tight coupling.

During the neutron transport for a certain time interval, the time-dependence of the temperature distribution was accounted for by linearly interpolating the temperature between the beginning-of-interval and end-of-interval temperature distributions based on the interaction time. The fuel behavior simulation used the integral power over the time interval divided by the time interval length as a constant power level throughout the interval, which did not account for the time-dependence of the power during the interval but did conserve the energy deposition.

A major shortcoming of the physics models in the demonstration simulation in Publication **III** was the lack of delayed neutron emission during the transient. Although the lack of a delayed neutron emission model for time-dependent simulations did not hinder the demonstration of the time-dependent coupled calculation routines, realistic transient simulations cannot be executed without such models. For this reason, new delayed neutron emission models were implemented for time-dependent simulations in Publication **IV** and verified against analytic solutions in infinite medium systems. The implementation utilized a delayed neutron group structure in the tracking of the delayed neutron precursors and in the various sampling routines used for, e.g. precursor production, delayed neutron emission time and energy. This group structure is generated automatically by the implementation based on the cross section libraries used in the simulation and the fissionable nuclides present in the modeled system. Some evaluated nuclear data libraries, such as ENDF/B libraries utilize a six group structure for the delayed neutrons, where the six groups are unique for each fissionable nuclide. JEFF libraries, however use eight groups that are common to all fissionable nuclides. The implementation uses a group structure, where each unique delayed neutron group is handled separately, meaning that simulations using JEFF based cross sections have eight delayed neutron groups and simulations using ENDF/B based cross sections have $6\times$(number of fissionable nuclides) groups. In Publication **IV** the models were not yet used for coupled calculations, but they have since been applied to both internally and externally coupled time-dependent simulations, although no results have yet been published.

7.5 Finalized unified coupling methodology

As the coupling approach between Serpent and coupled solvers, both internal and external, evolved during the thesis work, the last two publications focused on describing the final form of the coupling in steady state and burnup applications.

Publication **V** described the implementation of a unified coupling scheme used in both internally (Fig. 19) and externally (Fig. 20) coupled calculations for steady state applications. The stochastic approximation-based solution scheme (Algorithm 5)

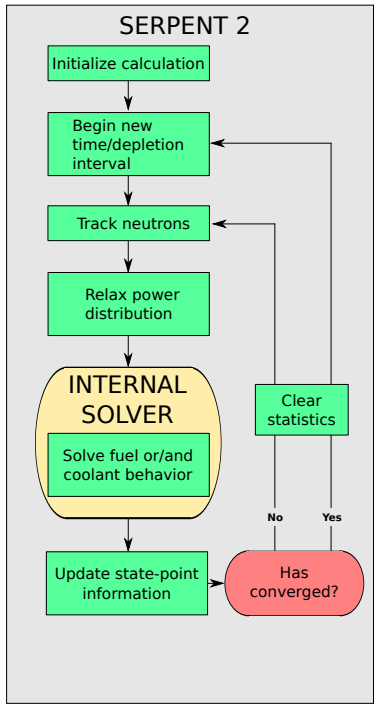

Figure 19. Solution flow in internally coupled calculations using the finalized coupled calculation routines.

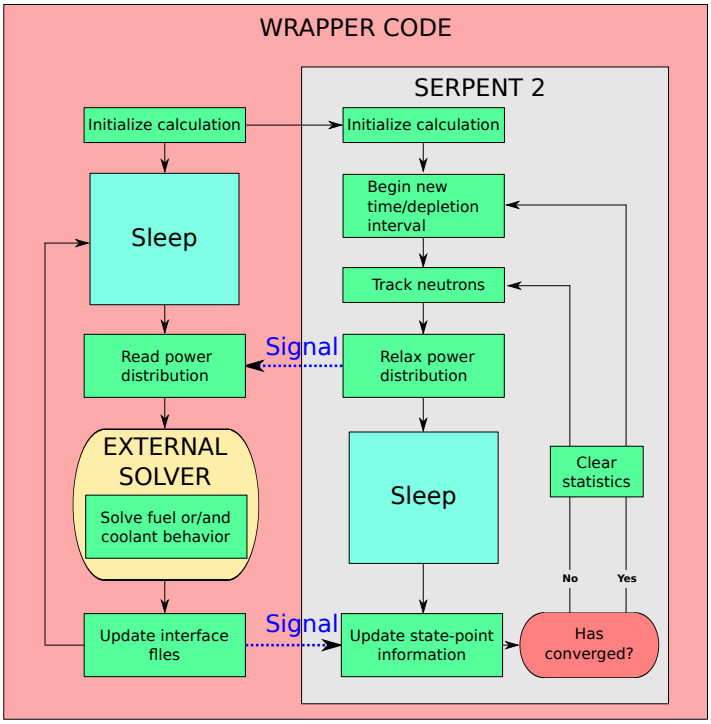

Figure 20. Solution flow in externally coupled calculations using the finalized coupled calculation routines.

was adopted in full for the solution relaxation. The finalized steady state capabilities were demonstrated in a coupled solution of neutronics and fuel behavior for a 3D BWR assembly geometry using both an internally and an externally coupled approach. Finally, Publication **VI** combined the steady state solution scheme used in the previous publication with the Stochastic Implicit Euler burnup scheme with thermal feedback [43] for coupled burnup calculations. The coupled burnup capabilities were applied to a series of 2D assembly burnup calculations using realistic fuel temperatures provided by the externally coupled ENIGMA fuel performance code.

At the end of the thesis project, the same coupling scheme (Figs. 19 and 20) can be used in steady state, burnup and transient calculations with internally or externally coupled solvers. Although the applications in this thesis were focused on fuel temperature coupling using the fuel behavior interface, the same coupled calculation approach can be used to couple any external solver with Serpent using one of the various multi-physics interface formats in Serpent. The coupled burnup calculations in Publication **VI** were conducted using the Stochastic Implicit Euler burnup scheme, but it is also possible to use the standard explicit Euler and predictor-corrector-based burnup schemes in Serpent with a stochastic approximation-based iteration for each neutron transport solution.

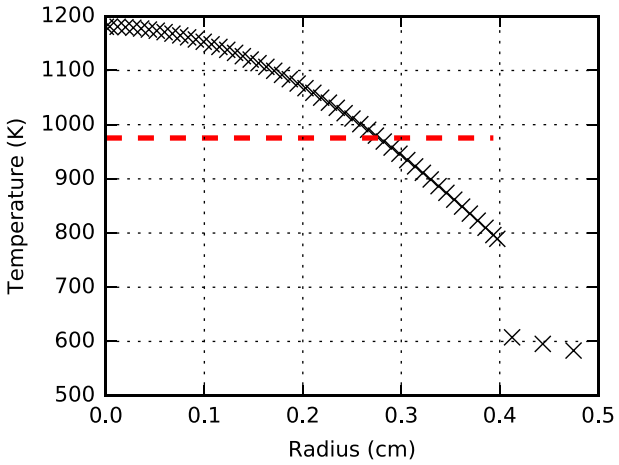

Figure 21. Realistic radial temperature distribution in fuel and in cladding at discrete nodes (x) and a radially constant effective fuel temperature (red dashed line) typically used in lattice calculations.

8. Application of the coupled calculation capabilities to effective fuel temperature problems

The multi-physics capabilities developed during this work were applied in Publications **I**, **II**, **V** and **VI**, partly as a demonstration, to the problem of effective fuel temperatures typically used in neutronics calculations. In order to understand this problem, consider the typical radial fuel temperature from the fuel rod centerline to the cladding outer surface shown in Fig. 21 with black x. Due to limitations in computational resources it is very common to run neutronics calculations using a single effective temperature (red dashed line) instead of a continuous temperature profile or a step profile [44]. As has been described previously in this thesis, the fuel temperature distribution has a strong effect on the neutronics of the system. The problem of the effective temperature is, then, how to choose the dashed line in Fig. 21 so that the neutron transport solution is preserved as well as possible.

The research into the optimal choice for this effective temperature has mostly focused on preserving the rate of resonance absorption in the system [45, 46, 47], i.e. choosing the effective temperature so that the number of neutrons lost to radiative capture by ^{238}U is conserved. Although the choice of an optimal effective temperature is generally a problem in multiple-objective optimization, the conservation of the radiative capture rate by ^{238}U is a good choice for an important objective, as it is the main basis of the fuel temperature reactivity feedback in low-enriched uranium. Moreover, conserving the radiative capture rate of ^{238}U should also automatically conserve the production rate for the fissile ^{239}Pu.

Several methods for calculating an estimate for this effective temperature have been used: A volume averaged fuel temperature is a simple and common approach to calculating an effective temperature, as was noted in [44]. Rowlands proposed already in [45] that the effective temperature should be calculated as the average temperature over all possible neutron track-lengths through the pellet, whereas Goltsev *et al.* suggested in [47] to use volume-averaging with an additional $1/\sqrt{T(r)}$ weighting function.

As the coupled calculation routines implemented in this work make it possible to use the accurate continuous fuel temperature profile even in large systems containing hundreds of fuel rods, it is possible to obtain accurate reference results for the effective temperature models (such comparisons were made in Publications **I**, **II** and **V**). Furthermore, the accurate flux solution obtained from the reference simulation can be used to accurately calculate various new effective temperatures. In Publication **V** this was demonstrated by calculating volume averaged effective temperatures using either the local collision rate or the local radiative capture rate as a weighting function.

8.1 Evaluating the performance of effective fuel temperature models in steady state calculations

The internal fuel temperature solver implemented in Publication **I** made it possible to obtain the accurate coupled neutronics–fuel temperature solution using the realistic continuous fuel temperature fields. In Publication **I** such a solution was obtained for a 2D BWR assembly geometry. The multiplication factor of the detailed solution was then compared to that of a simulation using an effective temperature obtained by volume averaging the accurate temperature solution over the total fuel volume of the assembly. The volume averaged effective temperature reproduced the reactivity of the assembly very well, leading to a reactivity difference of only 35 ± 4 pcm. However, the reactivity of the system is an integral parameter and does not give any indication of possible differences in local parameters.

Publication **V** applied a more robust evaluation of the effect of the effective radial fuel temperature by comparing three different pre-existing methods (Volume averaging, simplified Rowland's method and Goltsev's volume averaging with $1/\sqrt{T}$ weighting) and two new effective temperature models, that collapsed the realistic temperature distribution using volume averaging with local reaction rate weighting. The comparison was made against a reference solution using a realistic temperature profile at several axial levels of a 3D BWR assembly geometry. This time the comparison also included the differences in local reaction rates.

The main findings of publication **V**, with regard to effective fuel temperatures, can be summarized as follows: The radially constant effective fuel temperatures can reproduce the global radiative capture rate by ^{238}U rather well: The poorest performing effective temperature model led to a -0.20 % relative error in the global ^{238}U radiative capture rate. The global radiative capture rate was best reproduced by one of the novel effective temperature models, namely the ^{238}U radiative capture weighted effective temperature. However, all of the radially constant effective temperatures led to significant errors in the local reaction rates. With the use of effective temperatures, the radiative capture was overestimated in regions close to the pellet surface and underestimated in the pellet inner regions. This is explained by the fact

that the effective temperatures are significantly higher than the correct temperature at the pellet surface and significantly lower at the pellet center (see Fig. 21).

8.2 On the use of effective fuel temperatures in burnup calculations

The fact that large local differences in the capture reaction rates could be seen with the use of effective radial fuel temperatures prompted the question of possible effects on burnup calculations as differences in capture rates also indicate differences in the production of ^{239}Pu and other actinides. This was studied initially in publication **II** and later with the finalized coupled calculation routines in publication **VI**. Publication **VI** looked at the burnup effects in the context of generation of group constants for a core simulator for the simulation of the initial cycle of the EPR reactor [48], as briefly described in the following paragraphs.

The group constant generation for core simulators for a fuel cycle of a certain reactor consists of

1. a burnup calculation part to obtain the nuclide compositions for different fuel assemblies at different points of the fuel cycle and
2. a branch calculation part to generate the group constants using the nuclide compositions obtained from the burnup calculation.

It is quite normal to conduct the burnup calculation in the first part using a single effective temperature for all the fuel rods in the assembly. This not only ignores the radial variation in each fuel rod, but also does not consider the variation between the different fuel rods, which can be important if some of the fuel rods contain burnable absorber, which reduces their temperature by hundreds of Kelvin in the beginning of the fuel cycle.

The effects of the effective fuel temperature simplification on the local and assembly-wide nuclide inventories in the burnup calculation, as well as on the generated group constants and final core simulator results, was studied by generating one set of group constants using the traditional effective temperature approach for the history calculation and a second set of group constants by using realistic fuel rod and burnup-dependent radial temperature distributions in the burnup calculation. The realistic temperature distributions were obtained by coupling Serpent externally with the fuel performance code ENIGMA using the coupled calculation routines developed in this work.

The main findings of publication **VI** regarding the effective fuel temperatures were as follows: The use of the effective temperature resulted in a significant overestimation of the actinide production, fission power and thus fission product concentrations in the areas close to the fuel rod surface[10]. On the other hand, the same variables were underestimated for the fuel pellet inner regions, resulting on average in a conservation of the assembly-wide fission product concentrations. The results indicated that, with an optimal choice of the assembly-wide effective temperature, it may be possible to conserve reasonably well *either* the assembly-wide actinide concentrations *or* the gadolinium burnout from the burnable absorber (BA) rods. This suggests that it would be beneficial to use a separate effective temperature for the BA rods in the burnup calculation. The assembly-wise homogenized group

[10] Similar trends were also observed for the radial power distribution in Publication **II**.

constants were reproduced rather well by the effective temperature model and the effects on the simulation of the EPR initial cycle were minor. The study did indicate that the fuel temperature history of the fuel assemblies should be treated as an important history parameter in the parametrization of the cross sections for core simulators.

9. Future prospects

The last section of this manuscript will be devoted to describing some interesting prospects currently on the horizon for Monte Carlo multi-physics. The section is divided into two subsections, the first focuses on some possible upcoming methods and the second lists some possible future applications for the Monte Carlo multi-physics calculations.

9.1 Methodology

Although the coupled calculation capabilities implemented in this thesis allow the user to execute coupled steady state, burnup and transient calculations in a standardized manner, many possible avenues exist for the future development of the coupled calculation capabilities:

9.1.1 New algorithms for coupled burnup calculations

The coupled burnup scheme based on the Stochastic Implicit Euler method is known to have poor accuracy in applications that have rapid shifts in the neutron spectrum due to the reliance of the method on the use of end-of-step reaction rates [49]. Several improved techniques have already been proposed [50, 49, 51] and the search for efficient burnup algorithms for Monte Carlo applications is still ongoing. There is certainly a need to replace the SIE-based algorithm with a more efficient one, although it is not yet clear which algorithm will be the final choice for Monte Carlo multi-physics calculations.

9.1.2 Cheaper calculation of the Jacobian for Newton's method iteration

The history-based sensitivity and perturbation calculation methodology developed by Aufiero *et al.* [52] can be used to calculate the sensitivity of various results of the Monte Carlo simulation, such as the power distribution, to various input parameters such as nuclear data, material densities and material temperatures using a single Monte Carlo neutron transport simulation. For the Monte Carlo multi-physics problem, this means that the sensitivities required in the application of Newton's method could be obtained without the need to run hundreds or thousands of Monte Carlo neutron transport calculations. The methodology has already been applied to the calculation of the sensitivities in $k_{\text{eff.}}$ to the coolant density distribution in LFRs and SFRs [53]. Calculating the sensitivity of the power distribution tallied by the Monte Carlo code to the distributions provided by the coupled codes would pave the way for the possibility to couple Monte Carlo codes in a JFNK framework in an efficient manner.

9.1.3 Cheaper time-dependent calculations with hybrid methods

Time-dependent Monte Carlo neutron transport simulations are computationally expensive. Although the computational efficiency of the simulations may be improved using various methods for variance reduction [37], hybrid methods such as the Improved Quasi-Static (IQS) method [54] provide an attractive alternative due to the reduced computational effort. In the IQS method, the neutron flux solution is separated in space and time, at relatively short time intervals, into a time-independent flux shape and a space-independent flux-amplitude. By solving the time-independent flux shape after certain time intervals using detailed methods such as Monte Carlo neutronics, and leaving the time dependence to be solved by simplified methods such as the point-kinetics approximation, the computational effort is significantly reduced. The full Monte Carlo time-dependent capabilities can be used to verify the accuracy of the hybrid methods. The IQS method has already been implemented in the multi-group Monte Carlo code KENO [55] and in the three dimensional discrete ordinates code TORT [56].

9.1.4 Accurate calculation of the heat deposition

The simulations conducted in this work approximated the heat generation distribution in the simulated systems by assuming a nuclide dependent value for locally deposited heat due to each fission and no heat deposition to other materials due to direct neutron or photon heating. This was an acceptable approximation for the development and testing of the coupled calculation methodology, but it is a large simplification especially considering thermal-hydraulic calculations in which the heat generation in moderator, neutron absorbers and structural materials serves as a significant heat source.

The recent implementation of photoatomic interactions into Serpent [57] makes it possible to execute a photon transport simulations based on the results of a neutron transport calculation [58]. Using these capabilities, Serpent can calculate the direct heat deposition by both neutrons and photons as was demonstrated in [59]. By combining a separate model for the calculation of decay heat generated in the fuel, a more accurate representation for the power distribution could be calculated. Such an implementation will be of great use in future multi-physics calculations.

9.1.5 Delayed neutron group structure used in time dependent simulations

The delayed neutron emission routines implemented in Publication **IV** utilized a delayed neutron group structure in the handling of the delayed neutron precursors and in the sampling of the delayed neutrons. It would be possible, however, to do away with the group structure and instead tally each precursor nuclide separately. The production data for each nuclide can be obtained from the neutron induced fission yield data included in the evaluated nuclear data libraries and the data for the beta-decay of the precursors is present in the radioactive decay data in the libraries.

Tracking each delayed neutron precursor nuclide separately would most likely be costly in terms of memory demand, however it would make it possible to estimate the effects of the group structure approximation on time-dependent neutron transport

simulations. Another potentially interesting research direction would be the use of alternate delayed neutron group structures generated using the detailed data for each precursor nuclide separately and specifically for each simulation.

9.2 Applications

The obvious application for the Monte Carlo multi-physics capabilities is the production of accurate high-fidelity solutions to various coupled problems. Although the significant computational effort required for such calculations precludes the use of high-fidelity methods in day-to-day reactor analyses, the high-fidelity methods can be used to produce reference results for the fast reduced-order models used in the daily work.

Due to the versatility of the Monte Carlo method and the wide variety of input and output formats, it should be possible to use the same thermal-hydraulic solvers for the Monte Carlo solution and the reduced order solver. An example of such an application is given in [60], in which the neutronics solver in the code system DYN3D/SUBCHANFLOW, namely DYN3D, is benchmarked against the Seprent/SUBCHANFLOW code system. If the same Monte Carlo code is also used to generate the homogenized group constants for the reduced order solver, the differences related to cross section data libraries as well as to thermal hydraulic models can be eliminated.

Thus far, such comparisons have been made only for steady state simulations [60, 61], but time-dependent reference calculations for deterministic transient solvers are also possible, although the computational effort may limit the comparisons to relatively small and simple systems.

9.2.1 Novel options for group constant parametrization

The main development direction of Serpent has always been application of the code to the generation of spatially homogenized group constants for core simulators [62, 61, 63]. The traditional approach to modeling the fuel temperature feedback in the core simulator is to generate the group constants using several different flat fuel temperature profiles (for example at 600, 900 and 1200 K) and generating a functional expansion of the group constants with respect to the fuel temperature. During the execution of the core simulator, an assembly averaged effective fuel temperature is solved based on the assembly power and local thermal-hydraulic conditions. This effective temperature is then used to evaluate the group constants based on the functional expansion.

The flat homogeneous fuel temperature profiles used in the group constant generation do not correspond in a very meaningful way to the realistic fuel temperature profiles that would result from a certain node power/coolant temperature combination. Since the core simulator is usually only interested in the interaction properties for neutrons in the assembly at power P and coolant temperature T, the group constants could be directly generated for a set of node powers and coolant temperatures. With the new multi-physics capabilities, the group constant generation can use the realistic fuel temperature distribution corresponding to those conditions solved either by the Monte Carlo code or an external fuel behavior solver.

9.2.2 Detailed simulation of xenon transients

An interesting application for the developed coupled calculation routines would be the xenon transients that occur in PWR cores. Any perturbations to the power distribution will initiate a change in the concentrations in the concentrations of the short lived neutron absorber ^{135}Xe. The changes in the xenon concentrations will have an additional effect on the power distribution in the core with couplings to the fuel behavior and the thermal hydraulics. The xenon transients couple the time dependent neutronics with the time dependent fuel behavior, core level thermal hydraulics and fuel depletion (production and burning of ^{135}Xe).

The capability to model such complex transients with several interconnected couplings would serve as a formidable demonstrations of the coupled calculation capabilities of Serpent 2.

References

[1] IPCC, 2014: Climate change 2014: Mitigation of climate change. Contribution of working group III to the Fifth Assessment Report of the Intergovernmental Panel on Climate Change. Cambridge University Press, Cambridge, United Kingdom and New York, NY, USA.

[2] OECD-NEA, 2011: "Technical and economic aspects of load following with nuclear power plants", online report available at http://www.oecd-nea.org/ndd/reports/2011/load-following-npp.pdf.

[3] C. L. Waata. *Coupled Neutronics/Thermal-hydraulics Analysis of a High-Performance Light-Water Reactor Fuel Assembly*. PhD thesis, University of Stuttgart, 2006.

[4] V. Seker, J.W. Thomas, and T.J. Downar. Reactor simulation with coupled Monte Carlo and computational fluid dynamics. In *Proc. Joint International Topical Meeting on Mathematics and Computations and Supercomputing in Nuclear Applications, M and C + SNA 2007*, Monterey, California., 15–19 Apr. 2007.

[5] N. Capellan, J. Wilson, O. Méplan, J. Brizi, A. Bidaud, A. Nuttin, and P. Guillemin. 3D coupling of Monte Carlo neutronics and thermal-hydraulics calculations as a simulation tool for innovative reactor concepts. In *Proc. Global 2009*, Paris, France, Sept. 6–11 2009.

[6] A. Ivanov, V. Sanchez, and U. Imke. Development of a coupling scheme between MCNP5 and SUBCHANFLOW for the pin- and fuel assembly-wise simulation of LWR and innovative reactors. In *Proc. M&C 2011*, Rio de Janeiro, Brazil, May 8–12 2011.

[7] D. Kotlyar, Y. Shaposhnik, E. Fridman, and E. Shwageraus. Coupled neutronic thermo-hydraulic analysis of full PWR core with Monte-Carlo based BGCore system. *Nuclear Engineering and Design*, **241**, 3777–3786, 2011.

[8] Jaakko Leppänen, Maria Pusa, Tuomas Viitanen, Ville Valtavirta, and Toni Kaltiaisenaho. The Serpent Monte Carlo code: Status, development and applications in 2013. *Annals of Nuclear Energy*, **82**, 142 – 150, 2015.

[9] J. Lamarsh. *Introduction to Nuclear Engineering, Massachusetts (1983).* Addison-Wesley Publishing Company, Massachussets, 1983.

[10] Weston M. Stacey. *Nuclear Reactor Physics*. Wiley-VCH, 6 2007.

[11] Bernd Pfeiffer, Karl-Ludwig Kratz, and Peter Möller. Status of delayed-neutron precursor data: half-lives and neutron emission probabilities. *Progress in Nuclear Energy*, **41**, 39 – 69, 2002.

[12] R. E. Kelley and E. D. Clayton. Fissible: A proposed new term in nuclear engineering. *Letter to the Editor, Nucl. Sci. Eng.*, **91**, 481, 1985.

[13] L.W.G. Morgan and D. Kotlyar. Weighted-delta-tracking for Monte Carlo particle transport. *Annals of Nuclear Energy*, **85**, 1184 – 1188, 2015.

[14] E. Woodcock, T. Murphy, P. Hemmings, and S. Longworth. Techniques used in the GEM code for Monte Carlo neutronics calculations in reactors and other systems of complex geometry. Technical report, Argonne National Laboratory, 1965.

[15] W. A. Coleman. Mathematical verification of a certain Monte Carlo sampling technique and applications of the technique to radiation transport problems. *Nucl. Sci. Eng.*, **32**, 76–81, 1968.

[16] Massachussets Institute of Technology. Theory and methodology description of the OpenMC Monte Carlo code: https://mit-crpg.github.io/openmc/methods/physics.html, cited on 23 Nov. 2016.

[17] K. Ivanov et al. Benchmark for uncertainty analysis in modelling (UAM) for the design, operation and safety analysis of LWRs, volume I: Specification and support data for neutronics cases (Phase I). OECD/NEA, 2013.

[18] R. Pawlowski, R. Bartlett, N. Belcourt, R. Hooper, and R. Schmidt. A theory manual for multi-physics code coupling in LIME. Technical report, Sandia National Laboratories, 2011.

[19] D. A. Knoll and D. E. Keyes. Jacobian-free Newton–Krylov methods: a survey of approaches and applications. *J. Comput. Phys.*, **193**, 357, 2004.

[20] T.M. Evans, T.J. Urbatsch, H. Lichtenstein, and J.E. Morel. A residual Monte Carlo method for discrete thermal radiative diffusion. *Journal of Computational Physics*, **189**, 539 – 556, 2003.

[21] J. A. Willert, C. T. Kelley, D. A. Knoll, and H. Park. A hybrid approach to the neutron transport k-eigenvalue problem using NDA-based algorithms. In *Proc. M&C 2013*, Sun Valley, ID, 5–9 May 2013.

[22] Jeffrey Willert and H. Park. Residual Monte Carlo high-order solver for Moment-Based Accelerated Thermal Radiative Transfer equations. *Journal of Computational Physics*, **276**, 405 – 421, 2014.

[23] H. Robbins and S. Monro. A stochastic approximation method. *Ann. Math. Statist.*, **22**, 400, 1951.

[24] J. Dufek and W. Gudowski. Stochastic approximation for Monte Carlo calculation of steady-state conditions in thermal reactors. *Nuclear Science and Engineering*, **152**, 274 – 283, 2006.

[25] R. E. MacFarlane and D. W. Muir. *NJOY99.0 Code System for Producing Pointwise and Multigroup Neutron and Photon Cross Sections from ENDF/B Data*. PSR-480, Los Alamos National Laboratory, 2000.

[26] T. Trumbull. Treatment of nuclear data for transport problems containing detailed temperature distributions. *Nucl. Tech.*, **156**, 75, 2006.

[27] J. Donnelly. Interpolation of temperature-dependent nuclide data in MCNP. *Nucl. Sci. Eng.*, **168**, 180–184, 2011.

[28] S. Li, K. Wang, and G. Yu. Research on Fast-Doppler-Broadening of neutron cross sections. In *PHYSOR 2012*, Knoxville TN, Apr. 15-20, 2012.

[29] C. J. Dean, R. Perry, R. Neal, and A. Kyrieleis. Validation of run-time Doppler broadening in MONK with JEFF3.1. *J. Kor. Phys. Soc.*, **59**, 1162, 2011.

[30] Paul K. Romano and Timothy H. Trumbull. Comparison of algorithms for doppler broadening pointwise tabulated cross sections. *Annals of Nuclear Energy*, **75**, 358, 2015.

[31] W. R. M. G. Yesilyurt and F. B. Brown. On-the-fly Doppler broadening for Monte Carlo codes. *Nucl. Sci. Eng.*, **171**, 239 – 257, 2012.

[32] Benoit Forget, Sheng Xu, and Kord Smith. Direct Doppler broadening in Monte Carlo simulations using the multipole representation. *Ann. Nucl. Energy*, **64**, 78 – 85, 2014.

[33] T. Viitanen. *Development of a stochastic temperature treatment technique for Monte Carlo neutron tracking*. PhD thesis, Aalto University, 2015.

[34] T. Viitanen and J. Leppänen. Explicit treatment of thermal motion in continuous-energy Monte Carlo tracking routines. *Nucl. Sci. Eng.*, **171**, 165 – 173, 2012.

[35] J. Leppänen. Modeling of non-uniform density distributions in the Serpent 2 Monte Carlo code. *Nucl. Sci. Eng.*, **174**, 318, 2013.

[36] Matt Ellis, Benoit Forget, Kord Smith, and Derek Gaston. Preliminary coupling of the Monte Carlo code OpenMC and the Multiphysics Object-Oriented Simulation Environment (MOOSE) for analyzing Doppler feedback in Monte Carlo simulations. In *Proc. M&C + SNA + MC 2015*, Nashville, TN, 19–23 Apr. 2015.

[37] B. Sjenitzer. *The Dynamic Monte Carlo Method for Transient Analysis of Nuclear Reactors*. PhD thesis, Delft University of Technology, Delft, The Netherlands, 2013.

[38] J. Leppänen. Development of a dynamic simulation mode in Serpent 2 Monte Carlo code. In *Proc. M&C 2013*, Sun Valley, ID, 5–9 May 2013.

[39] J. Leppänen, T. Viitanen, and V. Valtavirta. Multi-physics coupling scheme in the Serpent 2 Monte Carlo code. *Trans. Am. Nucl. Soc.*, **107**, 1165, 2012.

[40] T. Ikonen, V. Tulkki, E. Syrjälahti, V. Valtavirta, and J. Leppänen. FINIX–fuel behavior model and interface for multiphysics applications. In *Proc. 2013 Fuel Performance Meeting TopFuel*, Charlotte, USA, 2013.

[41] Timo Ikonen, Henri Loukusa, Elina Syrjälahti, Ville Valtavirta, Jaakko Leppänen, and Ville Tulkki. Module for thermomechanical modeling of LWR fuel in multiphysics simulations. *Annals of Nuclear Energy*, **84**, 111 – 121, 2015.

[42] W. J. Kilgour, J. A. Turnbull, R. J. White, A. J. Bull, P. A. Jackson, and I. D. Palmer. Capabilities and validation of the ENIGMA fuel performance code. In *Proc. ANS/ENS Int. Topical Meeting on LWR Fuel Performance*, Avignon, France, 21–24 April 1991.

[43] J. Dufek and H. Anglart. Derivation of a stable coupling scheme for Monte Carlo burnup calculations with the thermal-hydraulic feedback. *Ann. Nucl. Energy*, **62**, 260, 2013.

[44] G. Grandi, K. Smith, Z. Xu, and J. Rhodes. Effect of CASMO-5 cross-section data and Doppler temperature definitions on LWR reactivity initiated accidents. In *PHYSOR 2010*, Pittsburgh, PA, May 9-14, 2010.

[45] G. Rowlands. Resonance absorption and non-uniform temperature distributions. *Journal of Nuclear Energy. Parts A/B. Reactor Science and Technology*, **16**(4), 235 – 236, 1962.

[46] W. J. M. De Kruijf and A. J. Janssen. The effective fuel temperature to be used for calculating resonance absorption in a 238UO2 lump with a nonuniform temperature profile. *Nuclear Science and Engineering*, **123**, 121 – 135, 1996.

[47] A.O. Goltsev, V.D. Davidenko, V.F. Tsibulsky, and A.A. Lekomtsev. Computational problems in the calculation of temperature effects for heterogeneous nuclear reactor unit cells. *Annals of Nuclear Energy*, **27**, 175 – 183, 2000.

[48] G. Sengler, F. Forêt, G. Schlosser, R. Lisdat, and S. Stelletta. EPR core design. *Nuclear Engineering and Design*, **187**, 79 – 119, 1999.

[49] D. Kotlyar and E. Shwageraus. Stochastic semi-implicit substep method for coupled depletion Monte-Carlo codes. *Annals of Nuclear Energy*, **92**, 52 – 60, 2016.

[50] D. Kotlyar and E. Shwageraus. Numerically stable Monte Carlo-burnup-thermal hydraulic coupling schemes. *Annals of Nuclear Energy*, **63**, 371 – 381, 2014.

[51] D. Kotlyar and E. Shwageraus. Sub-step methodology for coupled Monte Carlo depletion and thermal hydraulic codes. *Annals of Nuclear Energy*, **96**, 61 – 75, 2016.

[52] Manuele Aufiero, Adrien Bidaud, Mathieu Hursin, Jaakko Leppänen, Giuseppe Palmiotti, Sandro Pelloni, and Pablo Rubiolo. A collision history-based approach to sensitivity/perturbation calculations in the continuous energy Monte Carlo code SERPENT. *Annals of Nuclear Energy*, **85**, 245 – 258, 2015.

[53] Manuele Aufiero, Michael Vincent Martin, Massimiliano Fratoni, and Stefano Lorenzi. Analysis of the coolant density reactivity coefficient in LFRs and SFRs via Monte Carlo perturbation/sensitivity. In *Proc. PHYSOR 2016*, Sun Valley, ID, May USA, May 1–5 2016.

[54] Karl Ott. Quasistatic treatment of spatial phenomena in reactor dynamics. *Nucl. Sci. Eng.*, **26**, 563–565, 1966.

[55] K.L. Goluoglu, R. V. Demeglio, R. E. Pevey, I. Suslov, H. L. Dodds, C.L. Bentley, and S. Goluoglu. Application of TDKENO for analysis of criticality excursion experiments. *Transactions of the American Nuclear Society*, **78**, 145–146, 1998.

[56] S. Goluoglu and H. L. Dodds. A time-dependent, three-dimensional neutron transport methodology. *Nucl. Sci. Eng.*, **139**, 248–261, 2001.

[57] T. Kaltiaisenaho. Implementing a photon physics model in Serpent 2. Master's thesis, Aalto University, School of Science, 2016.

[58] J. Leppänen, T. Kaltiaisenaho, V. Valtavirta, and M. Metsälä. Development of a coupled neutron / photon transport mode in the Serpent 2 monte carlo code. In *M&C 2017*, Jeju, Korea, April 16-20 2017.

[59] M. Metsälä. Accurate heat deposition calculations in nuclear reactors using Monte Carlo neutron and photon transport. Special Assignment, Aalto University, School of Science, 2016.

[60] Miriam Knebel, Luigi Mercatali, Victor Sanchez, Robert Stieglitz, and Rafael Macian-Juan. Validation of the Serpent 2-DYNSUB code sequence using the Special Power Excursion Reactor Test III (SPERT III). *Annals of Nuclear Energy*, **91**, 79 – 91, 2016.

[61] Jaakko Leppänen and Riku Mattila. Validation of the Serpent–ARES code sequence using the MIT BEAVRS benchmark – HFP conditions and fuel cycle 1 simulations. *Annals of Nuclear Energy*, **96**, 324 – 331, 2016.

[62] Jaakko Leppänen, Riku Mattila, and Maria Pusa. Validation of the Serpent–ARES code sequence using the MIT BEAVRS benchmark – initial core at HZP conditions. *Annals of Nuclear Energy*, **69**, 212 – 225, 2014.

[63] Jaakko Leppänen, Maria Pusa, and Emil Fridman. Overview of methodology for spatial homogenization in the Serpent 2 Monte Carlo code. *Annals of Nuclear Energy*, **96**, 126 – 136, 2016.

[64] V. Valtavirta. Designing and implementing a temperature solver routine for Serpent. Master's thesis, Aalto University, School of Science, 2012.

[65] V. Valtavirta. Internal neutronics temperature coupling in Serpent 2 – reactivity differences resulting from choice of material property correlations. In *Proc. M&C 2013*, Sun Valley, ID, May 5–9 2013.

Errata

Publication **II**:
-The third sentence of section IV.A. ”The user input consists of a list of three variables, the cold condition radial coordinate of the point, the hot coordinate radial coordinate of the point and the temperature at the point” should read ”The user input consists of a list of three variables, the cold condition radial coordinate of the point, the hot *condition* radial coordinate of the point and the temperature at the point”.

Publication **III**:
-The first sentence of section 2.1 ”The dynamic simulation mode was implemented in an earlier version of Serpent 2, as an extension of the conventional time-dependent criticality source mode.” should read ”The dynamic simulation mode was implemented in an earlier version of Serpent 2, as an extension of the conventional time-dependent *external* source mode.”

-Two references show up as question marks in section 2.1. The intended references were [64] and [65].

-The first sentence of the third paragraph of section 2.2 starting ”The TMS-method was introduced for the first time in english-speaking journals...” should start ”The TMS-method was introduced for the first time in English-speaking journals...”

-The reader should note that the dashes in place of the authors’ names in the list of references indicate that the authors of that paper were the same as in the previous reference.

Publication **IV**:
-The reader should note that the dashes in place of the authors’ names in the list of references indicate that the authors of that paper were the same as in the previous reference.

Publication **V**:
-The denominator of Eq. 11 has an additonal $\phi(r)$ term. Moreover, the variable r is missing from both the numerator and denominator of Eqs. 11 and 12. The equations should thus read: Equation 11

$$T_{\text{eff.}} = \frac{\int_r T(r) r \mathrm{d}r}{\int_r r \mathrm{d}r}$$

and Equation 12:

$$T_{\text{eff.}} = \frac{\int_r w(r) T(r) r \mathrm{d}r}{\int_r w(r) r \mathrm{d}r}.$$

-In the first sentence of the first text paragraph on page 60, the symbol ^{283}U should read ^{238}U.

Aalto-DD 66/2017
VTT SCIENCE 150

ISBN 978-952-60-7377-4 (printed)
ISBN 978-952-60-7376-7 (pdf)
ISSN-L 1799-4934
ISSN 1799-4934 (printed)
ISSN 1799-4942 (pdf)

978-951-38-8530-4 (printed)
978-951-38-8529-8 (pdf)
2242-119X
2242-119X (printed)
2242-1203 (pdf)

Aalto University
School of Science
Department of Applied Physics
www.aalto.fi

BUSINESS + ECONOMY

ART + DESIGN + ARCHITECTURE

SCIENCE + TECHNOLOGY

CROSSOVER

DOCTORAL DISSERTATIONS